JOURNAL GEOLOGICAL SOCIETY OF INDIA
Vol.81, March 2013, pp.309-329

Petrogenesis of Ultramafic-Mafic to Felsic Plutonic Rock Associations from Southern Portion of Chhotanagpur Gneissic Complex in Central India: A Multi-stage Crust-mantle Interaction Process

KASTURI CHAKRABORTY[a] and ABHINABA ROY[b]
[a] Geological Survey of India, Southern Region
[b] Presidency University, Kolkata
Email: kasturi.8c@gmail.com

Abstract: A granite-granodiorite-gabbro-ultramafic rock association occurs in the southern sector of Chhotanagpur Gneissic Complex in Central India. Field relations show mingling and mixing of mafic and granodioritic magmas along the contacts of the intrusives. Petrographic studies, coupled with analyses of phase compositions and bulk rock major and trace element compositions favor origin of mafic magma from partial melting of sub-continental hybridized lithospheric mantle and subsequent two stage emplacement. Initial ponding of mafic magma at basal crust elevated the geothermal gradient so as to cause partial melting of lower crustal materials and generation of granodioritic melt. Simultaneous emplacement of granodioritic and mafic magmas tapped from basal crustal reservoir at mid-crustal depth resulted in restricted mingling-mixing along the contacts of the contrasting magma types locally producing rocks of dioritic composition. The mode of evolution of this cogenetic mafic-felsic association, when combined with available geochronological data, has important implications in demarcation of the extent of Grenvellian orogen that resulted in amalgamation of the Southern Crustal Province of India (SCP) with the Bundelkhand Craton or Northern Crustal Province (NCP).

Keywords: Granite-granodiorite-gabbro-ultramafic association, Magma mingling-mixing, Grenvellian orogen.

INTRODUCTION

The two major tectonic units in Central India are the Central Indian Tectonic Zone (CITZ) and the Chhotanagpur Gneiss Granulite Complex (CGC) separated by Gondwana sediments along the Mahanadi Graben. Both the units are presently believed to be amalgamations of a number of tectono-metamorphic terranes collaged through repeated tectonic reactivations (Roy and Prasad, 2003; Roy et al. 2006; Chatterjee and Ghose, 2011; Sanyal and Sengupta, 2012 and references therein). Based on structural patterns and geochronological evidences, many workers have questioned the separate identity of the twin terranes (Jain et al. 1995; Acharya, 2003; Chatterjee and Ghose, 2011; Sanyal and Sengupta, 2012). Rather, a continuity from Aravalli-Delhi orogen through CITZ and CGC into the sub-crop exposures of Bangladesh and Meghalaya has been suggested, thereby, presenting it as an extension of the ca.1.7-1.6 Ga old metamorphic belts of Albany-Fraser (Australia) and Windmill Island and Bunger Hills of Antarctica (Sanyal and Sengupta, 2012 and references therein). In this backdrop, the present work focuses on the tectono-magmatic evolution of a felsic-mafic rock association from the southern part of CGC and its comparability with evolutionary history recorded from southern CITZ.

The contribution of effective magma mixing between coeval mafic and felsic end member magmas towards generation of a hybrid magma had been another topic of much debate. Several workers have shown that although such hybridization processes can lead to generation of homogeneous hybrid magmas at depth, the volume of such magma should effectively be small, the hybridization process being constrained by a number of factors including viscosity of the individual magmas, crystallinity, relative viscosity, equilibrium temperature, mass fraction of the interacting magmas and time available for homogenization (Huppert et al. 1984; Frost and Mahood, 1987; Johnston and Wyllie, 1988; Neves and Vauchez, 1995; Wiebe et al. 2004; Barbarin, 2005; Jayananda et al. 2009). A more general result of partial interaction between magmas of contrasting composition is magma mingling leading to gradational contact between the intrusives and formation of mafic

0016-7622/2013-81-3-309/$ 1.00 © GEOL. SOC. INDIA

microgranular enclaves (Wiebe, 1991; Pitcher, 1991; Barbarin, 2005; Jayananda et al. 2009). Evidences of such magma mingling and development of mafic microgranular enclave (MME) have been reported from several parts of India including the Archaean granitoids in the Eastern Dharwar Craton (Jayananda et al. 2009), Neoproterozoic granitoids of south Khasi hills (Kumar et al. 2005) and Malanjkhand granite in Central India (Kumar et al. 2004, 2006). Mafic to hybrid microgranular enclaves (ME) and their field relation and microstructures with respect to felsic host has also been documented from the Ladakh granitoid of Ladakh batholith (Kumar, 2010). From the field and microstructural evidences he has suggested that the Ladakh granitoids and their microgranular enclaves are products of multistage magma mingling and mixing processes and concomittant fractional differentiation of several batches of mafic and felsic magmas formed in open magma chamber(s) of subducting setting. Here, we use a combination of field, textural, mineralogical and bulk rock geochemical data to infer the possible mode of evolution of ultramafic-mafic to felsic plutonic rock associations and local development of dioritic rocks by near complete homogenization of syn-plutonic basaltic and granitic magmas from the southern part of Chhotanagpur Gneissic Complex in Central India.

GEOLOGICAL SETTING

Bounded by the Bundelkhand craton in the north and the Baster and Singhbhum cratons in the south, the Precambrian CITZ-CGC belt has a complex tectono-magmatic history with granulites, supracrustal belts and vast areas of gneissic rocks. The CITZ is a college of several tectono-metamorphic terranes separated by large scale shear zones and deep faults viz. the Son-Narmada North Fault (SNNF), Son-Narmada South Fault (SNSF), Tan Shear Zone (TSZ) and the Central Indian Shear (CIS) from north to south (Jain et al, 1995; Roy and Prasad, 2003). In the east, the CITZ with its major tectonic features like TSZ and CIS, continues across the Mahanadi Graben into the CGC (Jain et. al., 1995). The CGC occupies approximately an area of 100,000 km^2 (~500 km long in E-W direction and 200 km in width) across the states of Chattisgarh, Jharkhand, Orissa and West Bengal of India (Ghose, 1992; Mahadevan, 2002; Acharyya, 2003; Sharma, 2009). The southern margin of the CGC is marked by an E-W to ENE-WSW trending crustal scale brittle to ductile shear zone, which, is commonly termed as Tamar-Porapahar - Khatra fault zone (TPKF, Mahadevan, 2002) or South Purulia Shear Zone (SPSZ, Majumdar, 1988). This shear/fault zone separates the CGC from the palaeo- to Mesoproterozoic North Singhbhum Fold Belt (NSFB) bordering the Archaean nucleus of Singhbhum craton (Fig.1.1B). Kinematic markers in the SPSZ indicate a north dipping thrust along, which rocks of the CGC are thrusted over the phyllitic rocks of the North Singhbhum Fold Belt (Majumdar and Chatterjee, 1990; Acharya et al. 2006). The CGC is bounded in the northwest by Mahakoshal Group and the Vindhyan sediments, in the north by Gangetic alluvium, in the east by Mesozoic Rajmahal trap basalt and by Gondwana deposits of Mahanadi Valley in

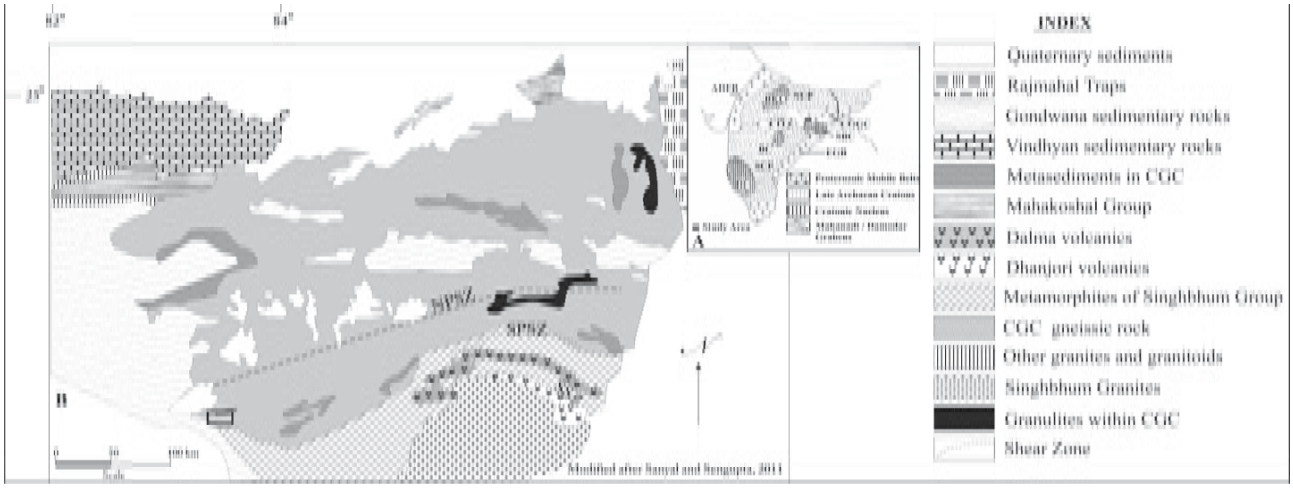

Fig 1.1. Geological map of Chhotonagpur Gneissic Complex (CGC), modified after Sanyal and Sengupta, 2011; the box at the south western part of the map shows the study area; inset clarifies position of CGC with respect to other tectonic units: Chhotonagpur Gneiss Granulite Complex (CGGC); Central Indian Tectonic Zone (CITZ); Bundelkhand Craton (BKC); Northern Crustal Province (NCP); Aravalli Delhi Fold Belt (ADFB); Baster Craton (BC); Dharwar Craton (DC); Southern Crustal Province (SCP); Eastern Ghat Belt (EGB); North Purulia Shear Zone (NPSZ); South Purulia Shear Zone (SPSZ); Singhbhum Shear Zone (SSZ).

the west (Fig.1.1B). Further extension of the terrane to the north and east beneath the Gangetic alluviam is suggested by the Gaya-Rajgir ridge and recent studies in Madhepur of Bangledesh (Hossain et al.2007; Chatterjee and Ghose, 2011).

The CGC comprises of extensive felsic gneisses and migmatites, enclaves of pelitic and mafic granulites, mica schist, metamorphosed dolomite and a host of intrusives presently represented by meta-gabbro, metadolerite, amphibolite, metamorphosed ultramafic rocks as well as anorthosite, granite, granodiorite, syenite, nepheline syenite, lamproite, pegmatite, alkaline lamprophyre and aplite (Ghose, 1983; Ghose, 1992; Ghose and Mukherjee, 2000; Ghose et al. 2005; Srivastava and Chalapati Rao, 2007; Mahadevan, 2008; Roy and Chakraborty, 2008; Chatterjee and Ghose, 2011). Based on available petrographic and geochronological evidences, Sanyal and Sengupta (2012) have classified the Precambrian tectono-metamorphic events in CGC into (1) a Palaeoproterozoic (>1.7 Ga) ultra-high temperature metamorphism leading to the development of the metapelitic and mafic granulites, (2) Mesoproterozoic intrusion of felsic magmas followed by their deformation, metamorphism and development of gneisses and migmatites, (3) 1.55-1.51 Ga intrusion of anorthosite into the gneisses, (4) Meso to Neoproterozoic (1.2-0.95 Ga) granulite grade metamorphism of the anorthosite, (5) intrusion of mafic magma into the high-grade basement at ~0.93 Ga, (6) green-schist to amphibolites facies metamorphism and deformation at ~0.90-0.85 Ga and (7) intrusion of post kinematic granite and pegmatite at ~0.85-0.80 Ga.

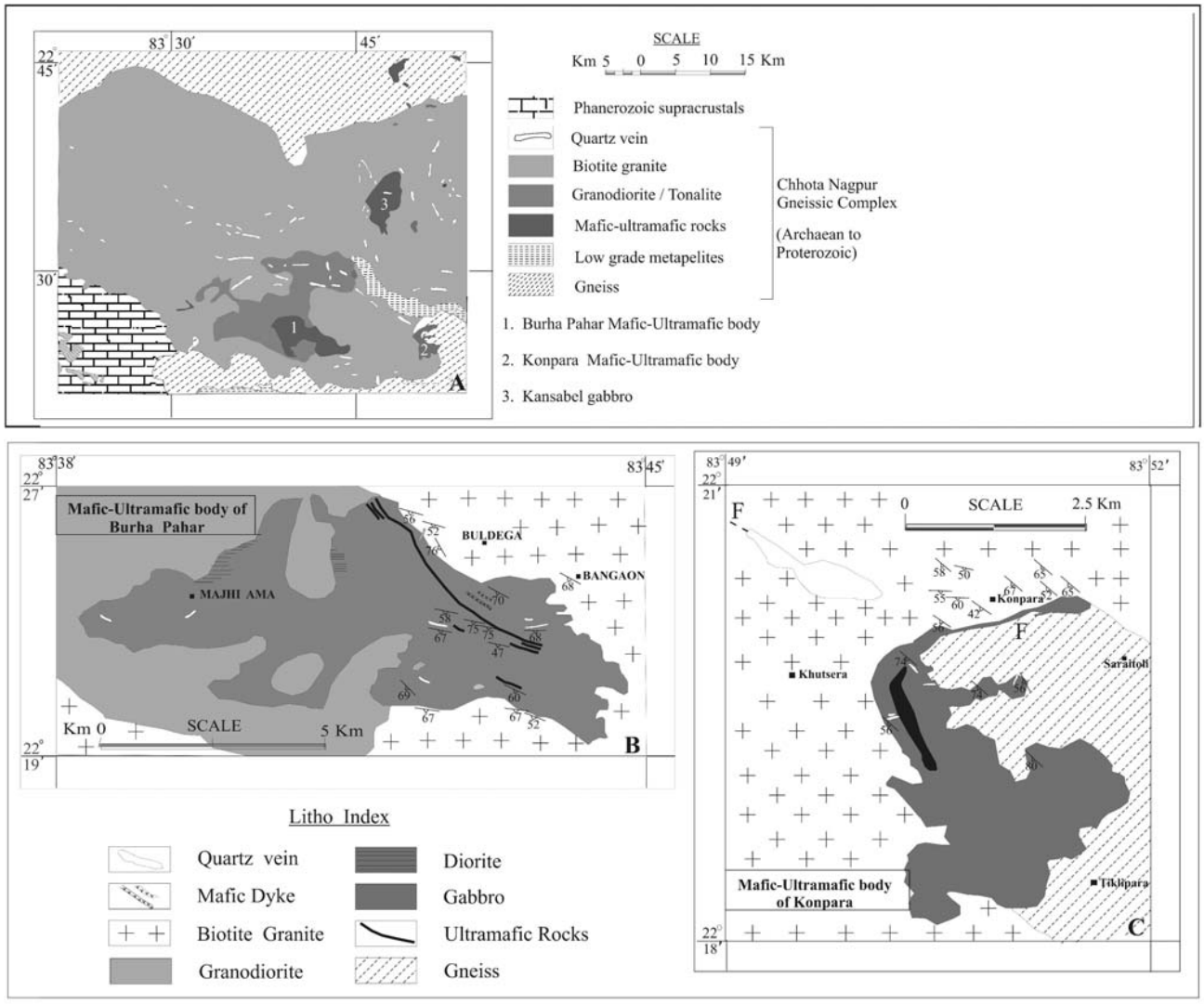

Fig 1.2. **(A)** General lithological map of the associated ultramafic-mafic-felsic intrusives within the study area in CGC; **(B)** The Burha Pahar mafic-ultramafic body and its associated granodiorite, diorite and granite; **(C)** The Konpara mafic-ultramafic body intrusive into the biotite gneiss of CGC.

Geology of the Study Area

A coarse to medium grained felsic biotite gneiss characterized by alternate biotite ± apatite bearing melanosomes and quartzofeldspathic leucosomes represents the oldest rock type in this area (Fig 1.2A) and is possibly the basement for the greenschist facies quartz muscovite schist (Roy and Chakraborty, 2008). Mafic-ultramafic, granodioritic and granitic rocks have intruded this gneissic basement.

Mafic-Ultramafic Rocks

There are a number of isolated hornblende-gabbro intrusives of varying dimensions together with subordinate volumes of ultramafics. The ultramafic rocks occur as narrow bands and lenses (a few meters across) within the hornblende gabbro, their contact with the later being gradational over a few centimeters (Fig 1.2B & C). Diorite occurs locally along the margins of the largest gabbro body in contact of adjoining granodioritic rocks. Contact between diorite and gabbro is gradational. Also at many places along the contact of granodiorite and gabbro, there occurs a variegated rock with irregularly distributed felsic and mafic patches of varying dimensions (Fig. 2a).

Granodiorite

Granodiorite occurs partially enveloping the largest mafic-ultramafic body (Burha Pahar) of the area (Fig. 1.2B). Enclaves of granodiorite occur within the mafic body whereas, enclaves of mafic rocks are present within the granodiorite. Magma-mingling along the contact of granodiorite with adjoining mafic rocks is evidenced locally by lobate and diffuse boundary between the two rock types (Fig.2b), occurrence of subparallel dismembered granodioritic and mafic bands (Fig. 2c and d) and occurrence of local small dioritic lenses with gradational contacts with both rock types. Closer to granodiorite, these rocks are locally constituted of hornblende and plagioclase along with epidote, chlorite, biotite and quartz. Although no direct contact exists between the mafic rocks and the metapelites, a xenolith of the later occurs within the gabbro near Konpara. A similar occurrence of quartz mica schist within

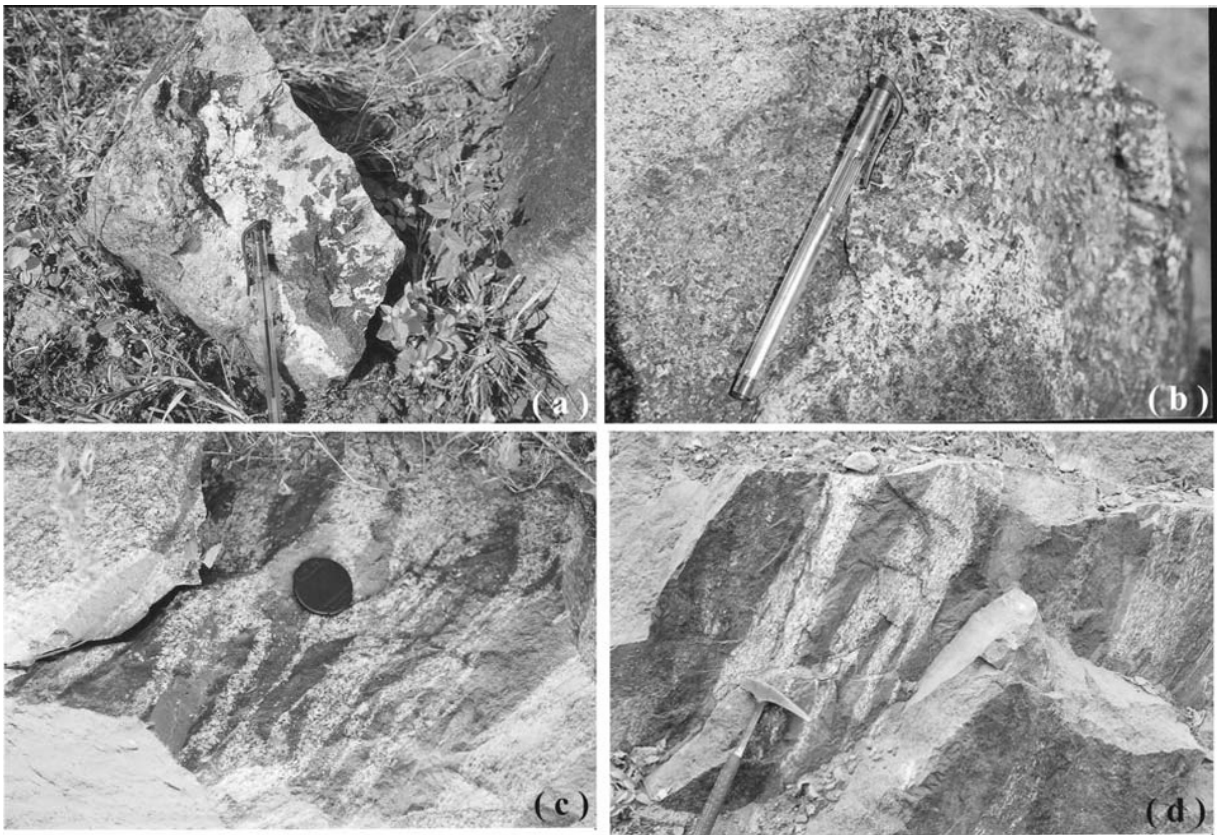

Fig.2. **(a)** Freshly broken rock sample from the spotted patchy/ variagated zone at the contact of gabbro and granodiorite showing hornblende-rich melanocratic and plagioclase-rich leucocratic patches. **(b)** Lobate and partly gradational boundary between mafic and granodioritic rocks. **(c)** Mafic inclusions within granodiorites. **(d)** Alternate bands of mafic and granodioritic rocks at the contact of gabbro and granodiorite.

amphibolite has been reported by Narang et al. (1983) near Kunkuri.

Biotite Granite

The third and by far the largest unit is a coarse grained grey biotite granite (Fig. 1.2). Enclaves of varying size, shape and composition occur within this unit, the most frequent among them being mafic rocks followed by schists and quartzite. The size of the mafic enclaves varies from a few centimeters to those of mapable dimensions. Xenoliths of metapelites and psammoites are more common in the central and northern parts of the area. Late pegmatites and quartz veins have intruded all the lithounits. Occurrence of several generations of quartz veins is evident from intensely sheared character of some and undeformed massive nature of the others. Rb-Sr age of ~ 1005±51 Ma has been reported by Singh and Krishna (2009) for similar grey granites occurring within a few kilometers of the study area (Raikera-Kunkuri area).

All the igneous rock types described so far are weakly deformed with marginal development of WNW trending foliation planes having moderate to steep south-westerly dip. Greenschist facies metamorphism is apparent in extensive development of actinolite and saussuritization of plagioclase in the mafic and ultramafic rocks. A number of local E-W trending shear zones have transected all the lithounits including the early generation of quartz veins.

PETROGRAPHY AND MINERAL CHEMISTRY

Analytical Procedures

The analyses were made using CEMECA Sx100 Electron Probe Micro Analyzer at the EPMA Laboratory, Central Petrological Laboratory, Geological Survey of India, Kolkata. The instrument was operated at 15 kV accelerating voltage, 1–2 micron beam diameter and 12 nA current. Natural standards were used for all the elements except for Mn and Ti for, which, synthetic standards were used. Bulk chemical analyses were carried out by PHILIPS X-ray Fluorescence at the Chemical Laboratory, Geological Survey of India, Central Region, Nagpur, while, rare earth elements were determined through Neutron Activation Analysis at Geological Survey of India, Pune. In the following sections some salient textural features and phase compositional characteristics of these rocks have been discussed.

Petrography and Mineral Chemistry of Mafic-Ultramafic Rocks

Mafic Rocks

The mafic rocks are gabbro to hornblende gabbro containing variable amounts of hornblende (45-65%, Table 1) and plagioclase (40-50%, Table 1), along with ilmenite and minor magnetite. The texture is dominantly hypidiomorphic although there are local ophitic to subophitic variants (Fig. 3a). Remnant clinopyroxenes are locally present within the hornblendes (Fig. 3b). Widespread imprints of fluid induced low grade metamorphism are apparent by actinolitic rims around pyroxene or hornblende or complete conversion of the phases to actinolite (Fig. 3a). Minor biotite and chlorite occur as alteration products of hornblende. Saussuritization of plagioclase is widespread. Deformation of the gabbro is restricted to narrow linear zones along the margins of the plutons where medium grained hornblendes have a strong preferred orientation (Fig. 3c). In the variegated rocks developed along the margins of gabbro and adjoining granodiorite, the leaucocratic patches contain entirely of coarse grained plagioclase whereas the melanocratic zones are dominantly of hornblende.

Clinopyroxenes are the most magnesian (Wo_{35-48} $En_{38-43}Fs_{14-21}$, Table 2.1) mineral in this rock. Their Al_2O_3 content of 1.88 to 3.97% can be explained by the CaTs ($CaAl_2SiO_6$) component in diopside. Amphiboles are by far the most abundant ferromagnesian phase and are dominantly magnesio-hornblende (X_{Mg} ~ 0.60-0.78, Table 2.2) although ferro-tschermakite (X_{Mg} ~ 0.43-0.52, Table 2.2) is present in the medium grained foliated gabbro. Actinolites have X_{Mg} ~ 0.64-0.76 (Table 2.2). Plagioclase is either unzoned or very small variations in anorthite content (2 to 4%) occurs from core to rim, the later being slightly richer in sodic component. They generally are andesine to labradorite in composition in the undeformed gabbros ($An_{54-69}Ab_{46-31}$, Table 2.3). In the variegated variety, however, the plagioclase is more calcic (X_{An} = 0.95).

Ultramafic Rocks

These are coarse grained highly altered cumulate rocks presently constituted dominantly of actinolitic amphiboles together with hornblende. Remnant clinopyroxene grains survive within fine grained actinolitic mass (Fig. 3d). Locally along deformed and foliated zones, the ultramafics have been completely altered to chlorite. Pressure solution cleavages transecting decussate medium grained chlorite indicate post metamorphic deformation (Fig. 3e). However, local lenses of unaltered ultramafics still survive within the gabbro. They are medium grained cumulate pyroxenites containing both subhedral clinopyroxene and subordinate coarser orthopyroxene (80-85% Cpx and 10-15% Opx, Fig. 3f, Table 1). Exsolution lamellae of clinopyroxene in ortho-pyroxene and vice versa are abundant. Plagioclase in minor amounts occur as an intercumulus phase (Fig. 3f).

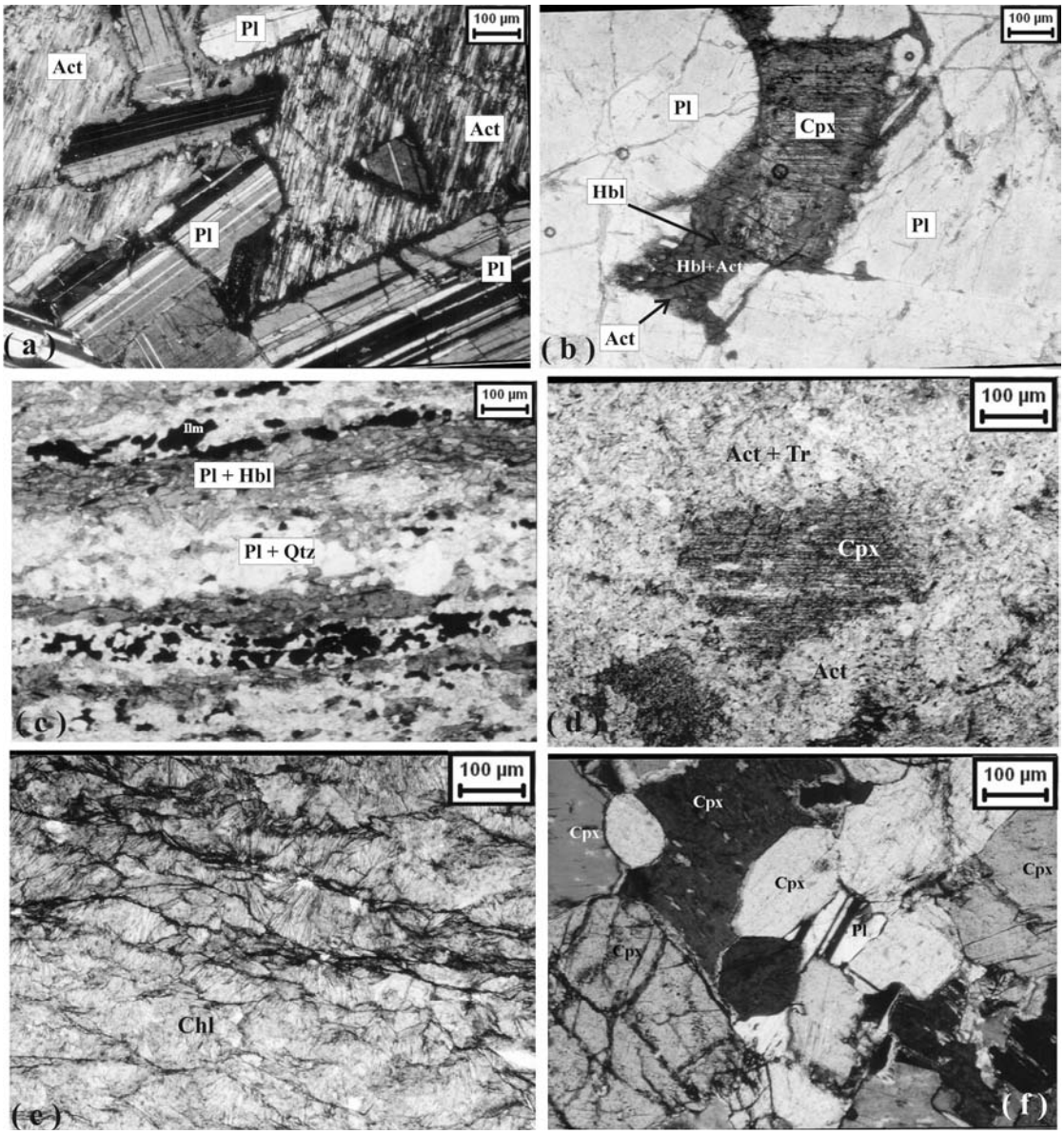

Fig 3. (a) Photomicrograph showing ophitic to subophitic texture with partially to completely included medium grained plagioclase laths within a coarse grained mafic phase that has been completely transformed into actinolite (crossed polars). **(b)** Remnant clinopyroxene within hornblende in gabbro (plane polarized). **(c)** Amphibolite with alternate hornblende-rich and feldspar-rich bands, hornblendes showing a strong preferred orientation (plane polarized). **(d)** Remnant clinopyroxene within fine grained actinolitie in altered pyroxenite. (plane polarized). **(e)** Complete chloritization of ultramafic rocks at the marginal part of Konpara mafic ultramafic bodies; the cleavages transect the randomly oriented chlorite grains (plane polarized) **(f)** Fresh pyroxenite with intercumulus plagioclase in relatively unaltered pyroxenite band (crossed nicols).

Hornblende is mainly a magnesio-hornblende (X_{Mg} ~0.73-0.82, Table 2.2). Tremolite-actinolite has X_{Mg} in the range of 0.88-0.91. Chlorite has X_{Mg} varying between 0.76 to 0.82 (Table 2.4). Unaltered and remnant clinopyroxene has composition in the range of $Wo_{42-49}En_{42-48}Fs_{7-14}$, while, orthopyroxene varies in the range $En_{74-77}Fs_{26-23}$. Intercumulus plagioclase is labradorite ($An_{74-78}Ab_{22-26}$) and is more or less homogeneous in composition.

Diorite

The diorite occurs locally along the contact of mafic rocks with adjoining granodiorite. The texture is inequigranular with altered coarse grained plagioclase phenocrysts in a groundmass of medium grained hornblende, plagioclase and minor ilmenite. The phenocrysts are characterized by oscillatory zoning.

Table 1. Modal composition of ultramafic rocks, gabbro, diorite, granodiorite and biotite granite

Constituent minerals	Ultramafic Rocks (fresh) (Pyroxinite)	Hornblende Gabbro	Diorite	Granodiorite	Biotite-granite
Px	80-85 % Cpx, 10-15 % Opx	Generally absent. Rarely Cpx present metastably in cores of hornblende.	none	none	none
Hbl	none	45-65 %	40-45 %	~ 10-15 %	generally absent, locally present as accessory.
Act	none	Replaces hornblende along the rims in partly altered samples, complete replacement of hornblende in highly altered samples.	Replaces hornblende along the rims in partly altered samples, complete replacement of hornblende in highly altered samples.	none	none
Pl	<8-10 %	40-50 %	50-55 %	30-40 %	~ 25-30 %
Bt	none	Minor, present as alteration product of Hbl in some samples	Minor, present as alteration product of Hbl in some samples	5-8 %, more abundant in the deformed varieties	8-10 %
Qtz	none	generally absent	<5 %	20-30 %	~ 35-45 %
Kfs	none	none	none	10-20 %	~ 30 %
Accessory minerals	Ilm, Mag	Mostly ilmenite, martitised magnetite, titanite, pyrite, chalcopyrite	Ilm, Mag	Epidote, magnetite, ilmenite, titanite	Hornblende, zircon, apatite
Other remarks		Chl at times occur as alteration product. In altered samples, plagioclase is epidotised, also patchy albitic replacement of plagioclase. Chalcopyrite has been partially altered to chalcocyte and covellite. Titanite generally forms rim around the ilmenite	Chl at times occur as alteration product. In altered samples, plagioclase is epidotised also patchy albitic replacement of plagioclase.	Plagioclase is epidotised, patchy albitic replacement of plagioclase is abundant	myrmekite along margins of plagioclase

Table 2.1. Representative major element analyses of pyroxene from ultramafic and mafic rocks of Pathalgaon

Phase	Cpx	Cpx	Cpx	Cpx	Opx	Opx	Opx	(Opx in Cpx(21))	(Cpx host to Opx 20)	Cpx	Cpx	Cpx	Cpx
Rock Type	UM (fr)	UM (fr)	UM (fr)	UM (fr)	UM (fr)	UM (fr)	UM (fr)	UM (fr)	UM (fr)	UM (alt)	UM (alt)	Gabbro	Gabbro
Sample No.	KK-1/a17 Core(16)	KK-1/a18 Rim(17)	KK-1/a37	KK-1/a44	KK-1/a1	KK-1/a12 (Rim 13)	KK-1/a13 (Core 12)	KK-1/a20 (exsoln)	KK-1/a21	S-10/a70 (Core 71)	S-10/a71 (Rim 70)	L-4/b89	L-4/b102
SiO_2	51.73	51.45	50.47	50.32	54.18	53.48	53.44	53.07	51.19	49.10	51.01	51.38	50.58
TiO_2	0.30	0.48	0.29	0.50	0.21	0.19	0.20	0.22	0.41	0.40	0.35	0.25	0.58
Al_2O_3	3.44	3.47	3.59	3.83	2.17	2.50	2.44	3.00	3.81	1.46	2.44	1.88	3.97
Cr_2O_3	0.72	0.62	0.65	0.58	0.30	0.43	0.46	0.35	0.63	1.23	0.68	0.04	0.05
FeO	5.76	6.16	5.36	6.50	12.16	13.52	13.09	18.17	5.15	7.14	4.11	8.80	12.47
MnO	0.21	0.30	0.11	0.03	0.21	0.18	0.29	0.32	0.16	0.21	0.20	0.16	0.21
MgO	16.10	15.51	15.23	16.36	28.90	28.28	27.21	25.08	15.27	15.26	15.54	13.09	14.09
CaO	21.06	21.65	22.54	20.00	1.02	0.93	2.76	1.30	21.96	23.57	23.96	23.33	16.02
Na_2O	0.48	0.45	0.40	0.37	0.04	0.01	0.04	0.09	0.49	0.06	0.19	0.29	0.36
K_2O	0.01	0.00	0.00	0.00	0.01	0.00	0.00	0.06	0.01	0.00	0.02	0.03	0.19
Total	**99.81**	**100.09**	**98.64**	**98.57**	**99.28**	**99.62**	**100.15**	**101.82**	**99.18**	**98.43**	**98.50**	**99.25**	**98.52**
Si	1.91	1.90	1.89	1.88	1.94	1.92	1.92	1.91	1.90	1.88	1.91	1.94	1.92
Ti	0.01	0.01	0.01	0.01	0.01	0.01	0.01	0.01	0.01	0.01	0.01	0.01	0.02
Al	0.15	0.15	0.16	0.17	0.09	0.11	0.10	0.13	0.17	0.07	0.11	0.08	0.18
Cr	0.02	0.02	0.02	0.02	0.01	0.01	0.01	0.01	0.02	0.04	0.02	0.00	0.00
Fe	0.18	0.19	0.17	0.20	0.36	0.41	0.39	0.55	0.16	0.23	0.13	0.28	0.40
Mn	0.01	0.01	0.00	0.00	0.01	0.01	0.01	0.01	0.01	0.01	0.01	0.01	0.01
Mg	0.88	0.85	0.85	0.91	1.54	1.52	1.46	1.35	0.84	0.87	0.87	0.74	0.80
Ca	0.83	0.86	0.90	0.80	0.04	0.04	0.11	0.05	0.87	0.96	0.96	0.94	0.65
Na	0.03	0.03	0.03	0.03	0.00	0.00	0.00	0.01	0.04	0.00	0.01	0.02	0.03
K	0.00	0.00	0.00	0.00	0.00	0.00	0.00	0.00	0.00	0.00	0.00	0.00	0.01
# Cation	4.02	4.02	4.03	4.03	4.01	4.01	4.02	4.02	4.02	0.42	0.44	4.02	4.00
$CaSiO_3$	0.44	0.45	0.47	0.42	0.02	0.02	0.05	0.03	0.47	0.47	0.49	0.48	0.35
X(Mg)	0.47	0.45	0.44	0.48	0.79	0.77	0.74	0.69	0.45	0.79	0.87	0.38	0.43

Normalized on the basis of 6 oxygen; UM(fr) - Fresh Ultramafic rock; UM(alt) - Altered Ultramafic rock; Gab. - Gabbro

Table 2.2. Representative major element analyses of hornblende from felsic and mafic rocks of Pathalgaon

Phase	Amp	Amp	Amp	Amp	Amp	Amp	Amp	Amp	Amp	Amp	Amp	Amp	Amp	Amp	Amp	Amp	Amp	Amp	Amp	Amp	Amp	Amp
Rock Type	GT	GT	GT	UM (alt)	UM (alt)	UM (alt)	UM (fr)	UM (fr)	UM (fr)	UM (alt)	UM (alt)	UM (fr)	Gabbro	Gabbro	Hbl-Gabbro	Hbl-Gabbro	Gabbro	Gabbro	Gabbro	Gabbro (foli)	Gabbro (foli)	Gabbro (foli)
Sample No.	L-10/43	L-10/32	L-10/44	S-10/a67	S-10/a69	S-10/a72	KK-4/b2	KK-1/a36	KK-4/b5	B-20/b65	B-20/b76	KK-4/b6	L-4/b93	L-4/b95	B-41/b131	B-41/b135	B-5/c3	B-5/c6 (Rc7)	B-5/c7 (Cc6)	B-69/b48	B-69/b58	S-37/b17
SiO_2	41.96	43.79	38.96	53.55	54.99	54.99	43.94	43.35	48.16	46.76	49.14	49.62	54.12	53.16	44.74	44.69	47.79	47	46.49	41.02	40.89	44.44
TiO_2	0.78	1.05	0.59	0.06	0.01	0.06	1.97	1.64	0.76	0.99	1.19	0.07	2.55	0.02	0.31	0.34	1.17	1.24	1.67	0.5	0.32	0.62
Al_2O_3	10.18	8.35	13.29	2.72	1.37	2.08	11.59	11.89	7.96	9.69	7.62	6.12	3.85	1.99	12.19	11.89	7.76	8.45	8.75	15.44	15.46	12.75
Cr_2O_3	0.00	0.01	0.05	0.24	0.02	0.15	1.58	0.95	1.25	0.26	0.22	0.9	0.13	0.09	0.02	0.05	0	0	0.03	0.01	0.05	0.00
FeO	21.03	19.49	22.05	5.25	4.78	5.55	8.69	7.74	7.94	10.74	9.19	9.52	11.12	10.64	13.68	13.93	12.87	13.01	11.63	19.00	19.31	17.51
MnO	0.64	0.63	0.68	0.2	0.2	0.08	0.11	0.08	0.11	0.14	0.09	0.15	0.27	0.08	0.33	0.2	0.31	0.27	0.18	0.32	0.23	0.22
MgO	7.55	8.56	6.20	20.08	20.72	20.38	14.61	15.05	16.05	14.36	16.75	16.57	14.02	16.72	10.81	11.01	13.95	13.38	14.63	7.01	7.12	9.17
CaO	11.34	11.64	11.57	13.46	13.37	13.43	12.30	12.36	12.54	12.42	12.27	12.76	11.91	12.63	12.48	12.38	12.19	12.5	11.92	11.78	11.99	11.96
Na_2O	1.21	0.96	1.24	0.33	0.23	0.32	1.80	1.93	0.98	1.18	0.89	0.76	0.36	0.22	1.09	0.98	0.71	0.77	0.95	1.36	1.39	0.99
K_2O	0.78	0.84	0.28	0.06	0.02	0.05	0.95	0.60	0.17	0.43	0.52	0.16	0.08	0.01	0.17	0.26	0.02	0.05	0.07	0.38	0.45	0.35
Total	**95.47**	**95.32**	**94.91**	**95.95**	**95.71**	**97.09**	**97.54**	**95.59**	**95.92**	**96.97**	**97.88**	**96.63**	**98.41**	**95.56**	**95.82**	**95.73**	**96.77**	**96.67**	**96.32**	**96.82**	**97.21**	**98.01**
^{T}Si	6.52	6.79	6.09	7.60	7.79	7.71	6.39	6.39	6.99	6.80	6.98	7.14	7.71	7.73	6.67	6.67	6.96	6.88	6.77	6.21	6.17	6.56
$^{T}Al^{(IV)}$	1.48	1.21	1.91	0.40	0.21	0.29	1.61	1.61	1.01	1.20	1.02	0.86	0.29	0.27	1.33	1.33	1.04	1.12	1.23	1.79	1.83	1.44
$^{C}Al^{(VI)}$	0.39	0.32	0.54	0.05	0.02	0.05	0.38	0.46	0.35	0.46	0.26	0.18	0.36	0.07	0.82	0.76	0.29	0.34	0.27	0.96	0.92	0.78
$^{C}Fe^{+3}$	0.50	0.26	0.66	0.16	0.09	0.10	0.06	0.07	0.10	0.16	0.28	0.35	-0.33	0.15	0.10	0.19	0.40	0.33	0.47	0.35	0.41	0.29
^{C}Ti	0.09	0.12	0.07	0.01	0.00	0.01	0.22	0.18	0.08	0.11	0.13	0.01	0.27	0.00	0.03	0.04	0.13	0.14	0.18	0.06	0.04	0.07
^{C}Cr	0.00	0.00	0.01	0.03	0.00	0.02	0.18	0.11	0.14	0.03	0.02	0.10	0.01	0.01	0.00	0.01	0.00	0.00	0.00	0.00	0.01	0.00
^{C}Mg	1.75	1.98	1.44	4.25	4.37	4.26	3.17	3.31	3.47	3.11	3.55	3.56	2.98	3.62	2.40	2.45	3.03	2.92	3.17	1.58	1.60	2.02
$^{C}Fe^{+2}$	2.24	2.27	2.22	0.46	0.48	0.55	0.99	0.87	0.85	1.14	0.76	0.80	1.65	1.14	1.61	1.55	1.16	1.27	0.91	2.06	2.03	1.84
^{C}Mn	0.03	0.05	0.06	0.02	0.02	0.01	0.00	0.00	0.00	0.00	0.00	0.00	0.03	0.00	0.04	0.02	0.00	0.02	0.00	0.00	0.00	0.00
^{B}Mg	0.00	0.00	0.00	0.00	0.00	0.00	0.00	0.00	0.00	0.00	0.00	0.00	0.00	0.00	0.00	0.00	0.00	0.00	0.00	0.00	0.00	0.00
$^{B}Fe^{+2}$	0.00	0.00	0.00	0.00	0.00	0.00	0.00	0.01	0.01	0.01	0.05	0.00	0.00	0.00	0.00	0.00	0.01	0.00	0.04	0.00	0.00	0.02
^{B}Mn	0.05	0.03	0.03	0.00	0.00	0.00	0.01	0.01	0.01	0.02	0.01	0.01	0.00	0.01	0.00	0.01	0.04	0.02	0.02	0.04	0.03	0.03
^{B}Ca	1.89	1.93	1.94	2.05	2.03	2.02	1.92	1.95	1.95	1.93	1.87	1.97	1.82	1.97	1.99	1.98	1.90	1.96	1.86	1.91	1.94	1.89
^{B}Na	0.06	0.04	0.03	0.00	0.00	0.00	0.07	0.03	0.03	0.03	0.07	0.02	0.10	0.02	0.00	0.01	0.05	0.02	0.08	0.05	0.03	0.06
^{A}Na	0.31	0.25	0.34	0.09	0.06	0.09	0.44	0.52	0.25	0.30	0.17	0.20	0.00	0.05	0.31	0.27	0.15	0.20	0.19	0.35	0.37	0.23
^{A}K	0.15	0.17	0.26	0.01	0.00	0.01	0.18	0.11	0.03	0.08	0.09	0.03	0.01	0.00	0.03	0.05	0.00	0.01	0.01	0.07	0.09	0.07
^{A}Ca	0.00	0.00	0.00	0.00	0.00	0.00	0.00	0.00	0.00	0.00	0.00	0.00	0.00	0.00	0.00	0.00	0.00	0.00	0.00	0.00	0.00	0.00
Total	**15.46**	**15.42**	**15.60**	**15.13**	**15.08**	**15.11**	**15.62**	**15.64**	**15.28**	**15.38**	**15.27**	**15.22**	**14.91**	**15.05**	**15.34**	**15.32**	**15.15**	**15.21**	**15.21**	**15.42**	**15.46**	**15.29**
X(Mg)	0.44	0.47	0.39	0.91	0.90	0.88	0.76	0.79	0.80	0.73	0.82	0.82	0.64	0.76	0.60	0.61	0.72	0.70	0.78	0.43	0.44	0.52
Amphibole Nomenclature	Ferrohornblende			Tremolite		Actinolite	Pargasite		Magnesiohornblende				Actinolite		Magnesiohornblende					Ferrotschermakite		

GT . Granodiorite UM. (fr) Fresh Ultramafic rock UM. (alt) Altered Ultramafic rock Gabbro (foli) Foliated Gabbro

Table 2.3. Representative major element analyses of feldspar from felsic and mafic rocks of Pathalgaon

Phase	(Pl)	(Pl)	(kfls)	(Pl)	(Pl)	(Pl)	(Pl)	(Pl)	(Pl)	(Pl)	(Pl)	(Pl)	(Pl)	(Pl)	(Pl)	(Pl)	(Pl)	(Pl)	(Pl)	(Pl)	(Pl)	(Pl)	(Pl)
Rock Type	Bt-Gr	Bt-Gr	Bt-Gr	GT	GT	GT	GT	GT	UM	UM	Gabbro	Gabbro	Gabbro	Gabbro	Gabbro	Gabbro	Gabbro	Gabbro	Gabbro	Gabbro	Gabbro	Gabbro (foli)	Gabbro (foli)
Sample No. (rim)	B-71-1 (core)	B-71-1	B-71-2 (rim)	L-10/1 (core)	L-10/1	L-10/28	L-10/30	L-10/35 (rim)	KK-1a (core)	KK-1a	L4/b113	L4/b114 (core)	L4/b96 (rim)	L4/b94 (core)	L4/b99 (rim)	L4/B100 (core)	L4/b104 (rim)	L4/b105 (core)	L4/b106 (rim)	L4/b107	L4/b109 (core)	B-69k (rim)	B-69k
SiO_2	65.14	67.14	62.52	57.86	54.93	57.86	54.93	56.85	49.48	48.25	54.01	51.39	51.40	50.04	50.31	52.06	49.99	51.01	50.82	50.78	50.60	46.83	54.87
TiO_2	0.00	0.00	0.00	0.00	0.00	0.00	0.00	0.00	0.04	0.03	0.00	0.02	0.08	0.01	0.03	0.07	0.05	0.00	0.00	0.04	0.04	0.00	0.03
Al_2O_3	20.34	20.41	17.93	26.01	27.39	26.01	27.39	26.29	32.01	32.81	28.77	31.16	30.34	30.05	30.82	30.25	31.22	30.45	30.79	30.93	30.38	33.82	28.47
Cr_2O_3	0.00	0.00	0.00	0.00	0.00	0.00	0.00	0.00	0.06	0.00	0.00	0.02	0.01	0.00	0.01	0.01	0.00	0.02	0.00	0.00	0.00	0.00	0.00
FeO	0.03	0.03	0.00	0.20	0.21	0.20	0.21	0.00	0.15	0.19	0.10	0.08	0.31	0.25	0.19	0.15	0.35	0.10	0.06	0.13	0.22	0.02	0.08
MnO	0.03	0.00	0.01	0.02	0.00	0.02	0.00	0.00	0.05	0.03	0.00	0.00	0.00	0.07	0.01	0.00	0.00	0.00	0.03	0.05	0.01	0.00	0.10
MgO	0.00	0.03	0.00	0.01	0.03	0.01	0.03	0.02	0.00	0.00	0.00	0.00	0.01	0.00	0.00	0.01	0.02	0.01	0.00	0.01	0.00	0.01	0.00
CaO	1.22	0.60	0.00	7.94	10.17	7.94	10.17	8.51	15.45	16.19	11.04	13.76	13.56	14.33	14.16	13.22	14.41	13.75	13.76	13.95	13.66	17.40	10.80
Na_2O	9.73	11.22	0.58	7.04	5.84	7.04	5.84	6.67	3.04	2.52	5.12	3.94	4.04	3.82	3.82	4.34	3.57	3.88	3.76	3.85	4.06	1.86	5.43
K_2O	1.65	0.22	16.45	0.08	0.07	0.08	0.07	0.07	0.03	0.05	0.06	0.06	0.08	0.05	0.03	0.05	0.05	0.02	0.03	0.03	0.05	0.01	0.05
Total	**98.14**	**99.66**	**97.77**	**99.60**	**98.69**	**99.16**	**98.64**	**98.41**	**100.31**	**100.07**	**99.10**	**100.43**	**99.83**	**98.62**	**99.38**	**100.16**	**99.66**	**99.24**	**99.25**	**99.77**	**99.02**	**99.95**	**99.83**
Si	2.93	2.95	2.98	2.61	2.51	2.61	2.51	2.59	2.26	2.21	2.46	2.33	2.34	2.32	2.31	2.36	2.29	2.34	2.33	2.32	2.33	2.15	2.48
Ti	0.00	0.00	0.00	0.00	0.00	0.00	0.00	0.00	0.00	0.00	0.00	0.00	0.00	0.00	0.00	0.00	0.00	0.00	0.00	0.00	0.00	0.00	0.00
Al	1.08	1.06	1.01	1.38	1.48	1.38	1.48	1.41	1.72	1.77	1.54	1.66	1.63	1.64	1.67	1.62	1.69	1.65	1.66	1.67	1.65	1.83	1.52
Cr	0.00	0.00	0.00	0.00	0.00	0.00	0.00	0.00	0.00	0.00	0.00	0.00	0.00	0.00	0.00	0.00	0.00	0.00	0.00	0.00	0.00	0.00	0.00
Fe	0.00	0.00	0.00	0.01	0.01	0.01	0.01	0.00	0.01	0.01	0.00	0.00	0.01	0.01	0.01	0.01	0.01	0.00	0.00	0.00	0.01	0.00	0.00
Mn	0.00	0.00	0.00	0.00	0.00	0.00	0.00	0.00	0.00	0.00	0.00	0.00	0.00	0.00	0.00	0.00	0.00	0.00	0.00	0.00	0.00	0.00	0.00
Mg	0.00	0.00	0.00	0.00	0.00	0.00	0.00	0.00	0.00	0.00	0.00	0.00	0.00	0.00	0.00	0.00	0.00	0.00	0.00	0.00	0.00	0.00	0.00
Ca	0.06	0.03	0.00	0.38	0.50	0.38	0.50	0.41	0.76	0.79	0.54	0.67	0.66	0.71	0.70	0.64	0.71	0.68	0.68	0.68	0.67	0.86	0.52
Na	0.85	0.96	0.05	0.62	0.52	0.62	0.52	0.59	0.27	0.22	0.45	0.35	0.36	0.34	0.34	0.38	0.32	0.34	0.33	0.34	0.36	0.17	0.48
K	0.09	0.01	1.00	0.00	0.00	0.00	0.00	0.00	0.00	0.00	0.00	0.00	0.00	0.00	0.00	0.00	0.00	0.00	0.00	0.00	0.00	0.00	0.00
# Cation	5.01	5.01	5.04	5.01	5.01	5.01	5.01	5.00	5.02	5.01	5.00	5.01	5.02	5.03	5.03	5.02	5.02	5.01	5.01	5.02	5.03	5.01	5.00
Xan	0.06	0.03	0.00	0.38	0.49	0.38	0.49	0.41	0.74	0.78	0.54	0.66	0.65	0.67	0.67	0.63	0.69	0.66	0.67	0.67	0.65	0.84	0.52
Xab	0.85	0.96	0.05	0.61	0.51	0.61	0.51	0.58	0.26	0.22	0.45	0.34	0.35	0.32	0.33	0.37	0.31	0.34	0.33	0.33	0.35	0.16	0.48
Xor	0.09	0.01	0.95	0.00	0.00	0.00	0.00	0.00	0.00	0.00	0.00	0.00	0.00	0.00	0.00	0.00	0.00	0.00	0.00	0.00	0.00	0.00	0.00

Normalized on the basis of 8 oxygen.

Bt-Gr Biotite-Granite GT . Granodiorite UM. (fr) Fresh Ultramafic rock UM. (alt) Altered Ultramafic rock Gabbro (foli) Foliated Gabbro

Petrography and Mineral Chemistry of Felsic Rocks

Granodiorite

This felsic unit is coarse grained and consists of variable amounts of quartz, plagioclase, K-feldspar, biotite and hornblende along with minor epidote, titanite, magnetite and apatite. The modal abundances of the major phases vary laterally (Table 1). Evidences of deformation are discernible with the development of anastomosing foliation planes defined by preferred alignment of medium grained biotite (X_{Mg} ~0.40, Table 2.4), hornblende (X_{Mg} ~0.39, Table 2.2) and titanite that truncate coarse, randomly oriented plagioclase ($An_{38-49}Ab_{51-61}$, Table 2.3) and ferro-hornblende (X_{Mg} ~0.44-0.47, Table 2.2) phenocrysts. Compositionally the plagioclase in granodiorite is andesine with 10 to 11% average decrease in the mole percent of anorthite from core to rim (Table 2.3). Saussuritization, epidotization and albitization are widespread. Anhedral quartz and K-feldspar occupy the interstices between plagioclase and hornblende phenocrysts.

Biotite Granite

Quartz, K-feldspar, sodic plagioclase and biotite are the dominant minerals in the biotite granite although subordinate hornblende, muscovite, epidote, zircon and apatite are also present. K-feldspar dominates over sodic plagioclase ($An_{3-6}Ab_{85-96}$, Table 2.3). Evidences of deformation are locally discernible with the development of foliation defined by preferred alignment of medium grained biotite (X_{Mg} ~0.09-0.19, Table 2.4) with minor muscovite. Myrmekites are present.

PHYSICAL CONDITIONS OF MAGMA EMPLACEMENT AND METAMORPHISM

Magma Emplacement

Table 3 summarizes the thermobarometric data. Experimental and theoretical studies have demonstrated that Al_2O_3 and TiO_2 contents of amphiboles coexisting with plagioclase and ilmenite/rutile can be potential geothermobarometers (Anderson and Smith, 1995; Earnst and Liu, 1998). In Fig.4a compositions of hornblendes from the mafic rocks, when plotted in the isoplethed (for Al_2O_3 and TiO_2) diagram of Earnst and Liu (1998), gives a maximum pressure limit of ~6 kbar at a temperature range of 680-840ºC. The lower values possibly represent reequilibriation during later metamorphism. Using the 'Al in Hornblende'-barometer (Anderson and Smith, 1995) is rendered difficult due to absence of the complete buffering assemblage (quartz + alkali feldspar + plagioclase + hornblende + biotite + iron titanium oxide + titanite + melt + fluid, Johnson and Rutherford, 1989; Thomas and Ernst, 1990; Schmidt, 1992) in the mafic rocks. The associated granodiorite (containing the full buffering assemblage) yields pressure in the range of 5.4-5.8 kbar. The hornblende-plagioclase thermometer (Holland and Blundy, 1994), when

Table 2.4. Representative major element analyses of minerals from felsic and mafic rocks of Pathalgaon

Phase	Bt	Bt	Bt	Bt	Bt	Bt	Bt	Bt	(Ilm)	(Ilm)	(Chl)	(Chl)	(Chl)	(Chl)
Rock Type	GT	GT	GT	Bt-Gr	Bt-Gr	Bt-Gr	UM (alt)	Gabbro	Gabbro	Gabbro	UM (alt)	Hbl-Gabbro	UM(foli)	UM(foli)
Sample No.	L10/34	L10/35	L10/36	B71/26	B71/27	B71/28	B20	B41	B-69/b54	B-69/b55	S-10/a68	B-41/b127	B-85/c20	B-85/c22
SiO_2	33.62	34.32	34.31	34.85	35.97	35.84	36.79	38.27	0.08	0.00	29.53	26.10	27.07	26.95
TiO_2	1.70	2.05	1.91	2.51	2.36	2.53	0.43	1.87	52.15	52.39	0.03	0.03	0.04	0.07
Al_2O_3	16.24	17.66	17.25	18.32	18.62	18.35	14.66	16.48	0.02	0.00	18.08	20.85	21.42	22.25
Cr_2O_3	0.00	0.14	0.19	0.00	0	0.00	0.35	0.22	0.00	0.00	0.53	0.05	0.00	0.00
FeO	23.12	21.56	21.82	28.26	25.98	24.32	5.98	12.16	45.40	44.22	10.70	18.80	13.09	12.35
MnO	0.41	0.19	0.09	0.30	0.21	0.19	0.11	0.18	1.93	2.19	0.19	0.27	0.14	0.15
MgO	8.68	8.08	8.23	1.64	2.87	3.14	25.98	16.32	0.09	0.02	26.97	19.19	23.63	24.30
CaO	0.01	0.02	0.02	0.05	0.26	0.28	0.13	0.09	0.04	0.03	0.10	0.15	0.00	0.03
Na_2O	0.06	0.07	0.08	0.03	0.09	0.07	0.45	0.41	0.00	0.03	0.04	0.22	0.00	0.01
K_2O	8.49	9.24	9.35	9.85	9.51	9.72	7.22	8.75	0.00	0.00	0.00	0.04	0.00	0.00
Total	92.33	93.33	93.25	95.81	95.87	94.44	92.1	94.75	99.71	98.88	86.17	85.70	85.39	86.11
Si	2.71	2.71	2.72	2.77	2.81	2.82	2.71	2.82	0.00	0.00	5.85	5.45	5.48	5.39
Ti	0.10	0.12	0.11	0.15	0.14	0.15	0.02	0.10	1.99	2.01	0.00	0.00	0.01	0.01
Al	1.54	1.64	1.61	1.71	1.71	1.70	1.27	1.43	0.00	0.00	4.22	5.13	5.11	5.24
Cr	0.00	0.01	0.01	0.00	0.00	0.00	0.02	0.01	0.00	0.00	0.08	0.01	0.00	0.00
Fe	1.56	1.42	1.45	1.88	1.69	1.60	0.37	0.75	1.92	1.89	1.77	3.28	2.22	2.06
Mn	0.03	0.01	0.01	0.02	0.01	0.01	0.01	0.01	0.08	0.09	0.03	0.05	0.02	0.03
Mg	1.04	0.95	0.97	0.19	0.33	0.37	2.85	1.79	0.01	0.00	7.96	5.97	7.13	7.24
Ca	0.00	0.00	0.00	0.00	0.02	0.02	0.01	0.01	0.00	0.00	0.02	0.03	0.00	0.01
Na	0.01	0.01	0.01	0.00	0.01	0.01	0.06	0.06	0.00	0.00	0.02	0.09	0.00	0.00
K	0.87	0.93	0.94	1.00	0.95	0.98	0.68	0.82	0.00	0.00	0.00	0.01	0.00	0.00
#Cations	7.86	7.81	7.84	7.73	7.68	7.67	8.00	7.80	4.01	3.99	19.96	20.03	19.96	19.98
X(Mg)	0.40	0.40	0.40	0.09	0.16	0.19	0.88	0.70			0.82	0.64	0.76	0.78

Normalized on the basis of 11 oxygen. Bt-Gr Biotite-Granite; GT - Granodiorite; UM.(alt)- Altered Ultramafic rock; UM. (foli) - Foliated chloritized ultramafics

Table 3. Thermobarometric data from felsic and mafic rocks of Pathalgaon

Sample No.	Rock-type	Al in Hbl (Anderson and Smith, 1995)		Hbl-Pl thermometer (Holland and Blundy, 1994)		Two Pyroxene thermometer (Kretz, 1982)
		Temperature Input (in °C)	Pressure deduced (in kbar)	Pressure Input (in kbar)	Temperature deduced (in °C)	
L10/44	Granodiorite	800	5.8			
L10/43	Granodiorite	800	5.4			
L10/44	Granodiorite			5.8	820.4	
L10/43	Granodiorite			5.4	824.8	
L10/59	Granodiorite			5.0	818.2	
S37/b20	Amphibolite			5.0	673.4	
B69/43	Amphibolite			5.0	653.7	
B69/62	Amphibolite			5.0	722.5	
S37/b17	Amphibolite			5.0	703.9	
S37/b22	Amphibolite			5.0	637.7	
KK-1/C16/O15	Pyroxenite					1180.4
KK-1/C18/O19	Pyroxenite					1214.8
KK-1/C40/O38	Pyroxenite					1195.7
KK-1/C44/O42	Pyroxenite					1205.2
KK-1/C47/O48	Pyroxenite					1115.0

applied to the granodiorites, gives temperature of ~820 ºC (Table 3). Two-pyroxene thermometer (Kretz, 1982), applied to the unaltered pyroxenites, yielded temperatures in the range of ~1180 ± 50ºC (Table 3). Many of the pyroxene grains have exsolution lamellae. Figure 4b is a plot of the reintegrated composition of these pyroxenes in a pyroxene ternary quadrilateral having isotherms at 5 kbar (Lindsley, 1987). Both the orthopyroxenes and the clinopyroxenes cluster between 1150-1250 ºC isotherms, which, in all possibility, represents the temperature of crystallization of the pyroxenes.

Geothermobarometric data, thus indicate emplacement of a hydrous basaltic magma at pressure between 4-6 kbar with initial temperature of 1200 ºC. For granodiorites, the emplacement pressure was 5.4-5.8 kbar and the temperature ~ 820 ºC.

Metamorphism

Hornblende-plagiocalse thermometry (Holland and Blundy, 1994) involving mineral pairs from the strongly foliated margin of gabbro bodies (Fig. 3c) yield recrystallization temperature of about 680±50ºC (Table 3). Pressure of < 4 kbar was derived from Al-in-hornblende barometry (1.4 to 3.7 kbar, Anderson and Smith, 1995). However, the widespread actinolite formation and abundant saussuritization of plagioclase are indicative of yet lower temperature.

GEOCHEMISTRY

Major Element Geochemistry

Representative major and trace element chemistry of the rocks has been presented in Table 4. AFM plot (after Irvine and Baragar, 1971) shows a distinct compositional gap between the felsic and mafic rocks with the former having calc-alkaline character and the later showing tholeiitic trend (Fig. 5.1a). The biotite granites, however, are far more alkalic compared to the granodiorites. A compositional gap is also reflected in the plot of wt% K_2O vs wt% SiO_2 (Fig. 5.1b), which, includes the field boundaries of Peccerillo and Taylor (1976). Here, the ultramafic to intermediate rocks plot in the field of tholeiite, granodiorites are high K-calc alkaline, while, granites have much higher K_2O and SiO_2 content. The calc-alkalic character of the granodiorites and granites is once again confirmed by the Na-K-Ca triangular plot (Fig. 5.1c) of Berker and Arth (1976). Separate trends for felsic and mafic series are also apparent in the wt % MgO vs wt % SiO_2 and wt % Al_2O_3 vs wt % SiO_2 Harker variation diagrams (Fig. 5.2a & d). The degree of alumina saturation in the rocks is demonstrated in the molar A/CNK vs SiO_2 plot (Fig. 5.1d) where the mafic-ultramafic rocks cluster in the metaluminous field (A/CNK_{molar} ~ 0.17-0.50 for ultramafic rocks and ~ 0.42-0.93 for mafic to intermediate rocks), while, granites and granodiorites plot in 'peraluminous' field, with the later straddling into the field of metaluminous rocks (A/CNK_{molar} ~ 1.08-1.25 for granites and ~ 0.75-1.27 for granodiorite). Diorite, although dominantly peraluminous, also extend into the metaluminous field. Magnesium number [(Mg/Mg+Fe)*100] for the ultramafic, mafic and dioritic rocks ranges in the order of ~53-72, ~31-58 and ~20-41 respectively. Also difference in range of magnesium-number demarcates mafic / ultramafic rocks from different bodies (~ 63-71 for Konpara and ~ 54-57 for Burha Pahar) and reflects either heterogeneity in source or different degrees of partial melting or both.

Negative trend in the X_{MgO} vs Al_2O_3 (Fig 5.3a) and initial

Table 4. Representative major and trace element composition for ultramafic rocks, gabbros, granodiorites, biotite-granite and host gneisses

Rock Type	Bt-Gr	Bt-Gr	GT	GT	GT	GT	GT	UM (alt)	UM (alt)	UM (alt)	UM (alt)	UM (alt)	UM (alt)	UM (alt)	Gabbro (foli)	Gabbro	Gabbro	Gabbro	Gabbro	Gabbro	Gabbro	Gabbro	Diorite	Diorite	Diorite	Diorite
S. No.	B-04	B-73	S-50	S-51	S-55	B-74	B-76	S-10	S-14	S-42A	B-06	B-20	B-22	B-52	S-37	L-04	L-13	L-07	B-05	B-10	B-24	B-41	B-13	B-15	B-18	B-45
SiO_2	72.33	73.68	67.02	64.08	66.98	62.43	62.07	49.86	51.50	57.05	48.22	49.80	51.42	45.93	51.17	46.70	39.71	48.91	45.10	49.93	56.63	45.48	46.48	63.02	57.54	65.54
TiO_2	0.02	0.06	0.28	0.32	0.25	0.51	0.03	0.41	0.76	0.58	0.34	0.29	0.32	0.37	1.98	0.33	1.83	0.26	0.85	0.63	0.64	0.77	0.74	0.58	0.56	0.71
Al_2O_3	14.10	14.20	16.91	16.23	15.81	14.46	16.15	4.18	3.12	1.93	5.40	3.33	4.17	6.04	13.25	16.30	15.47	10.53	8.66	8.37	14.52	10.53	12.51	12.55	13.28	13.35
$FeO^{(t)}$	2.38	1.99	2.38	2.49	2.21	5.21	4.35	8.36	10.57	10.95	13.63	13.88	13.53	15.12	13.47	7.70	16.27	10.86	15.97	11.54	9.12	13.53	13.21	6.55	8.73	5.58
MnO	0.05	0.03	0.06	0.06	0.07	0.08	0.02	0.20	0.21	0.14	0.22	0.24	0.26	0.23	0.16	0.15	0.22	0.18	0.23	0.22	0.15	0.20	0.24	0.11	0.15	0.11
MgO	0.27	0.20	0.84	0.94	0.67	2.70	0.29	21.10	20.58	18.85	17.87	18.62	16.46	19.88	6.19	9.65	7.71	15.23	12.93	13.09	5.10	12.45	9.34	3.04	5.84	1.37
CaO	0.51	0.88	2.30	2.36	2.17	4.51	4.62	13.50	4.66	4.33	8.11	6.36	7.75	6.10	9.98	13.00	12.03	7.72	9.38	10.21	6.95	10.60	9.91	5.80	6.87	5.16
Na_2O	3.45	3.64	3.74	3.63	4.30	3.08	4.30	0.29	0.31	0.22	0.50	0.24	0.28	0.48	1.10	1.54	1.12	1.37	0.55	0.76	2.05	0.70	1.18	1.89	2.38	2.12
K_2O	5.97	5.08	3.94	3.82	3.98	1.59	2.37	0.03	0.04	0.02	0.08	0.05	0.11	0.08	0.42	0.15	0.76	0.09	0.11	0.15	1.00	0.23	0.28	0.19	0.31	0.11
P_2O_5	0.03	0.04	0.15	0.13	0.14	0.20	0.01	0.02	0.02	0.03	0.04	0.02	0.02	0.04	0.25	0.02	0.86	0.02	0.09	0.11	0.15	0.03	0.12	0.22	0.13	0.26
LOI	1.98	0.52	1.46	1.44	0.14	1.00	2.74	1.81	2.62	3.76	2.89	3.50	2.97	4.49	0.61	1.23	2.18	2.45	2.70	2.15	2.34	2.19	2.59	2.70	1.84	1.94
Total	101.09	100.32	99.08	95.50	96.72	95.77	96.95	100.69	100.23	99.08	98.82	97.88	98.80	100.44	100.08	97.63	99.97	98.83	98.35	98.44	99.67	98.22	98.07	97.38	98.60	96.87
Mg-no	10.17	9.13	26.05	27.39	23.24	34.13	6.25	71.62	66.08	63.25	56.73	57.29	54.88	56.81	31.48	55.61	32.15	58.37	44.74	53.16	35.85	47.92	41.42	31.70	40.09	19.72
Nb	17.00	14.00	12.00	11.00	8.00	10.00	6.00	1.00	2.00	13.00	5.00	10.00	4.00	3.00	11.00	1.00	2.00	2.00	3.00	5.00	7.00	3.00	1.00	5.00	9.00	10.00
Zr	25.00	56.00	113.00	134.00	132.00	120.00	64.00	21.00	33.00	57.00	37.00	58.00	30.00	45.00	156.00	15.00	30.00	12.00	22.00	59.00	118.00	23.00	37.00	95.00	61.00	92.00
Y	9.00	12.00	24.00	11.00	19.00	14.00	15.00	9.00	15.00	17.00	5.00	18.00	14.00	6.00	25.00	13.00	31.00	5.00	11.00	53.00	16.00	11.00	22.00	12.00	27.00	6.00
Sr	31.00	78.00	170.00	220.00	151.00	250.00	164.00	15.00	12.00	13.00	96.00	24.00	88.00	41.00	514.00	245.00	305.00	213.00	173.00	157.00	298.00	232.00	257.00	300.00	317.00	524.00
Rb	90.00	70.00	146.00	127.00	166.00	57.00	28.00	2.00	3.00	2.00	4.00	2.00	3.00	2.00	9.00	2.00	32.00	2.00	2.00	3.00	34.00	2.00	4.00	4.00	9.00	2.00
Zn	17.00	15.00	nd	nd	nd	nd	nd	45.00	141.00	94.00	85.00	80.00	92.00	131.00	15.00	46.00	140.00	70.00	116.00	121.00	70.00	86.00	115.00	50.00	78.00	56.00
Ni	4.00	2.00	nd	nd	nd	nd	nd	385.00	424.00	1074.00	135.00	126.00	91.00	148.00	55.00	76.00	27.00	123.00	71.00	138.00	25.00	65.00	27.00	14.00	28.00	6.00
Co	92.00	87.00	nd	nd	nd	nd	nd	72.00	65.00	80.00	80.00	59.00	54.00	83.00	63.00	51.00	40.00	65.00	61.00	66.00	43.00	47.00	47.00	69.00	64.00	99.00
Cr	11.00	5.00	17.00	10.00	7.00	17.00	7.00	5113.00	1647.00	2122.00	319.00	465.00	434.00	448.00	48.00	252.00	111.00	192.00	183.00	363.00	353.00	159.00	32.00	13.00	43.00	13.00
Ba	770.00	990.00	740.00	910.00	570.00	480.00	330.00	250.00	260.00	252.00	259.00	238.00	262.00	247.00	366.00	254.00	384.00	254.00	268.00	288.00	381.00	253.00	281.00	281.00	293.00	293.00
La	28.80	30.00	41.00	30.00	35.00	26.00	5.90	1.30	2.10	2.50	3.20	2.00	3.00	7.00	28.00	2.50	14.00	1.20	3.20	14.00	16.00	2.00	8.30	10.00	19.00	25.00
Ce	62.00	77.00	80.00	63.00	51.00	39.05	13.00	3.00	5.00	6.10	7.30	4.50	6.40	16.00	65.00	5.10	32.00	3.10	7.60	32.00	32.00	4.50	18.00	16.00	30.00	43.00
Nd	6.20	18.00	30.00	16.00	19.00	12.00	7.20	1.90	3.30	4.10	4.60	3.00	4.10	8.00	27.00	3.30	20.00	2.30	5.00	20.00	12.00	3.00	11.00	6.86	12.00	19.00
Sm	2.20	2.80	4.90	3.70	4.00	2.80	1.80	0.56	1.00	1.30	1.10	1.10	1.20	9.60	5.80	0.91	4.90	0.74	1.30	5.30	2.20	0.89	3.10	1.20	3.00	4.20
Eu	0.29	0.80	5.40	1.10	0.70	0.96	0.61	0.26	0.37	0.46	0.37	0.37	0.37	0.64	1.80	0.32	1.80	0.28	0.46	1.80	0.60	0.32	1.10	1.20	1.00	1.30
Tb	0.34	0.30	1.82	1.45	1.05	1.01	0.38	0.16	0.30	0.24	0.20	0.28	0.14	0.17	0.66	0.21	0.87	0.22	0.29	0.82	0.35	0.28	0.97	0.24	0.94	0.57
Yb	0.81	0.63	3.2	2.96	2.49	2.30	0.83	0.57	1.06	0.87	0.81	1.04	0.51	0.64	2.52	0.85	3.12	0.82	1.08	3.15	1.34	1.00	2.94	0.66	2.92	1.84
Lu	0.10	0.08	0.40	0.38	0.30	0.28	0.10	0.08	0.16	0.14	0.12	0.16	0.08	0.10	0.41	0.12	0.45	0.12	0.16	0.48	0.20	0.14	0.40	0.09	0.40	0.25
Th	8.00	9.00	12.40	10.60	12.50	7.90	1.60	2.10	2.30	0.13	0.47	2.40	0.30	1.09	1.90	2.30	0.10	0.25	0.32	0.56	2.00	0.41	0.61	3.30	2.90	0.81
Sc	3.00	1.90	6.00	6.00	6.00	19.00	1.89	76.00	39.00	16.00	65.00	82.00	98.00	30.00	33.00	62.00	65.00	37.00	70.00	65.00	36.00	76.00	64.00	23.00	34.00	17.00
Hf	1.30	1.20	2.40	2.20	1.50	4.20	1.50	0.35	0.88	0.69	0.33	0.36	0.10	0.70	5.26	0.53	2.20	0.28	0.42	0.63	2.60	0.23	2.20	3.50	0.95	11.60

Bt-Gr: Biotite-Granite, GT: Granodiorite-tonalite, Gabbro (foli): Foliated Gabbro,Gabbro (foli): Foliated Gabbro, UM. (fr): Fresh Ultramafic rock, UM. (alt): Altered Ultramafic rock

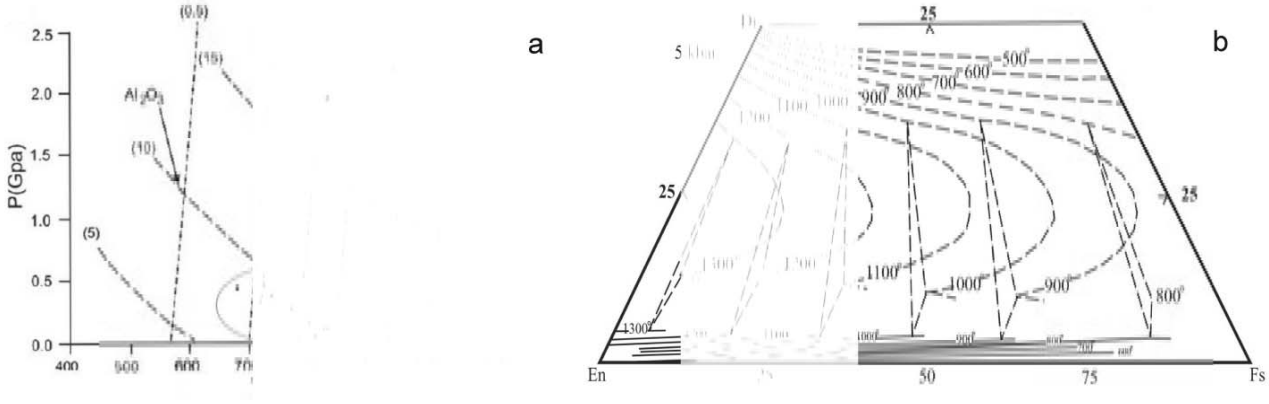

Fig.4. **(a)** Plots of amphibole composition in the isoplethed (for Al_2O_3 and TiO_2) diagram of Earnst and Liu (1998). **(b)** Plots of reintegrated pyroxene compositions on a pyroxene ternary quadrilateral having isotherms at 5 kbar (Lindsley, 1987); the grey patches represent the compositions of reintegrated orthopyroxenes and clinopyroxenes.

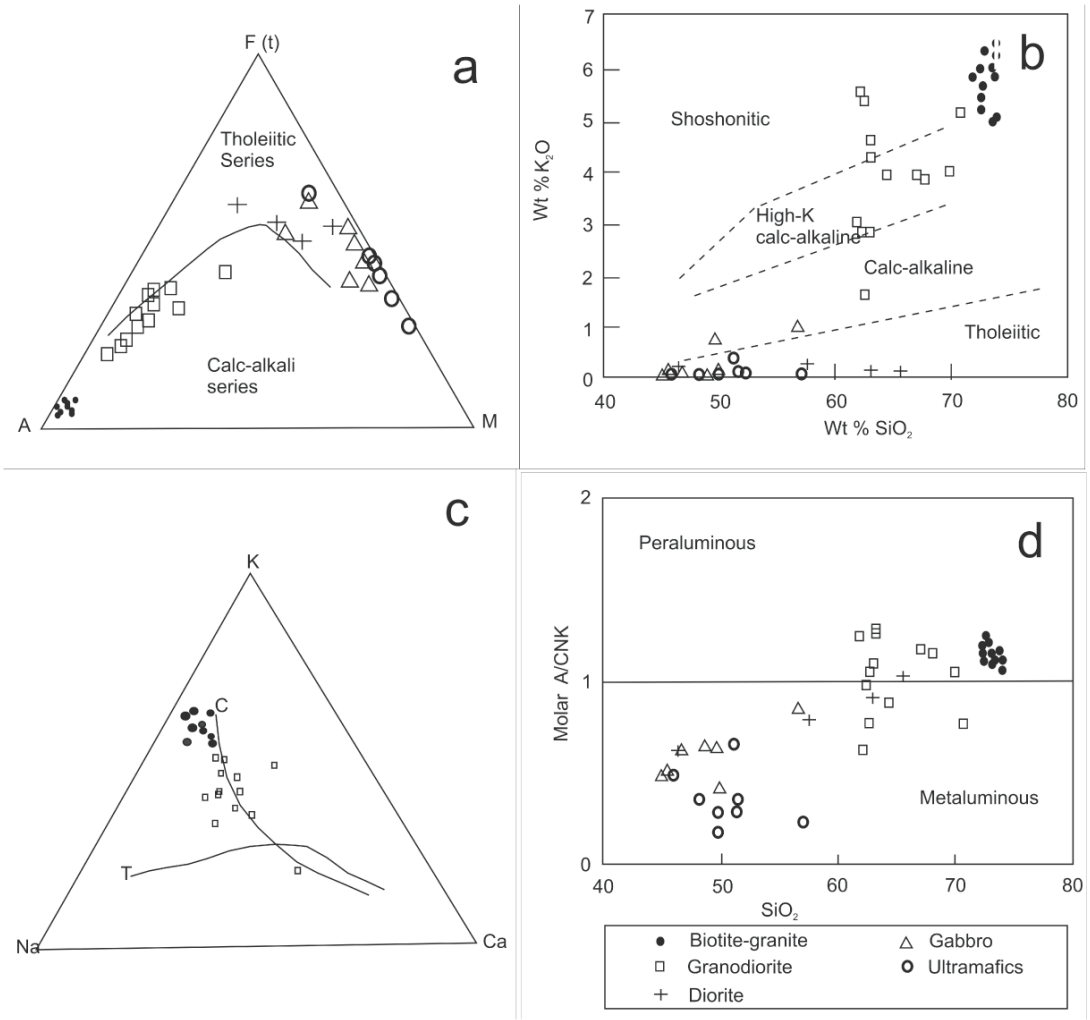

Fig 5.1. **(a)** AFM plot for ultramafic, mafic, intermediate and felsic intrusives of Pathalgaon area (with the boundary between calc alkaline and tholeiitic fields after Irvine and Baragar, 1971). **(b)** Wight % K_2O vs weight % SiO_2 plot of ultramafic, mafic, intermediate and felsic bulk compositions; superposed are the field boundaries of Peccerillo and Taylor (1976). **(c)** Na-K Ca triangular classification diagram (Berker and Arth, 1976) for granodiorites and biotite-granites. **(d)** Degree of alumina saturation in the ultramafic, mafic, dioritic, granodioritic and granitic rocks.

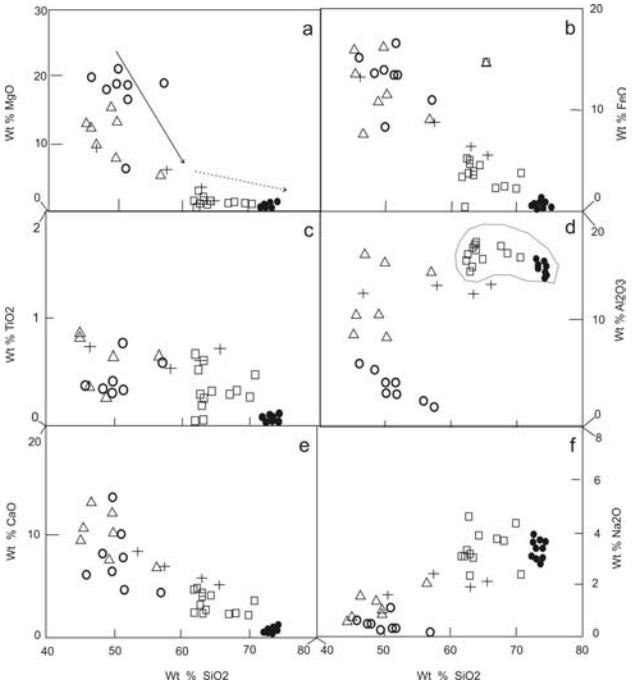

Fig.5.2. Harker variation diagrams showing variations in MgO, FeO, TiO_2, Al_2O_3, CaO and Na_2O with increasing SiO_2 for the ultramafic, mafic, dioritic, granodioritic and granitic rocks from Pathalgaon area (symbols as in Fig 5.1).

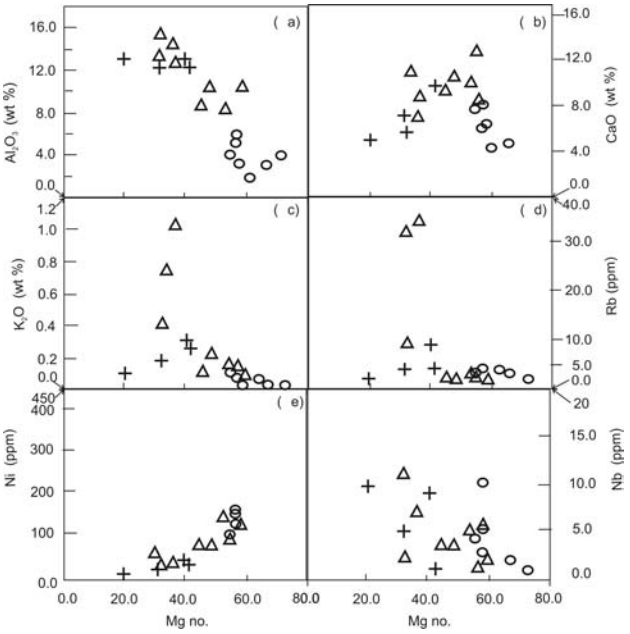

Fig.5.3. Variations in Al_2O_3 (wt %), CaO (wt %), K_2O (wt %), Rb (ppm), Ni (ppm) and Nb (ppm) against Mg no. for the ultramafic, mafic and dioritic rocks from Pathalgaon area (symbols as in Fig 5.1).

negative trend in X_{MgO} vs CaO diagrams (Fig. 5.3b) for the mafic-ultramafic and dioritic rocks confirm accumulation of orthopyroxene and clinopyroxene followed by plagioclase. Although the distribution of K_2O with respect to X_{MgO} have an overall negative trend, two of the gabbro samples show anomalously high K-content, which, might possibly be attributed to crustal contamination (Fig. 5.3c).

Trace Element Geochemistry

A few representative data that have been presented in Table 4 reveal that the Konpara mafics and ultramafics are richer in Cr and Ni and poorer in Sr as compared to Burha Pahar. Lack of any discernible pattern in plots of Zr vs Ni (Fig 6.1a) and Zr vs Cr (Fig. 6.1b) indicates that neither olivine nor spinel was fractionated from the magma. In contrast, negative trend in Zr vs Sc plot (Fig. 6.1c) was caused through pyroxene fractionation. Calculation of Rayleigh fractionation with partition coefficients for mafic rocks (Arth, 1976) shows that approximately 10% fractionation of pyroxenes (85% clinopyroxene with 15% orthopyroxene as in the studied rocks) could have caused the observed trend in trace element distribution pattern. Similarly, a cumulate origin for the ultramafic rocks is suggested from Fig. 6.1d which presents the Rayleigh fractionation pattern for Ni vs Cr. The vectors suggest that 10% fractional crystallization of either hornblende or pyroxene from magma with composition broadly similar to the gabbro could lead to the observed distribution array of mafic-ultramafic rocks. Similar fractionation can explain the mafic-ultramafic trend in Ni-Sr plot (Fig 6.1e). Such observation is also supported by the volumetric proportion of ultramafic to mafic rocks observed in the field.

A compositional gap between the felsic and mafic series is well apparent in both the Ni-Sr (Fig. 6.1e) and Rb-Sr (Fig. 6.1f) diagrams. Two gabbro samples in Fig 6.1f and Fig 5.3d show higher Rb content but they form a part of the linear array in X_{MgO} vs compatible elements like Ni (Fig. 5.3e) and Nb (Fig. 5.3f). Such local enrichment of incompatible elements in proportions much higher than the general array can be attributed to inhomogeneous crustal contamination.

The primitive mantle normalized trace element distribution pattern of mafic, ultramafic, dioritic and granodioritic rocks have been presented in Fig.6.2 (a-d). Higher proportions of K, Rb and Zr in three gabbro samples collected from marginal parts of the pluton are also reflected in primitive mantle normalized plot (Fig.6.2a, dashed lines), whereas, the other gabbro samples show more consistent pattern with much lower concentrations of K and Rb. Such local enrichment of elements like K, R and Zr in only a few marginal gabbros indicates possible contamination through fluid flux. This is further supported by location of these

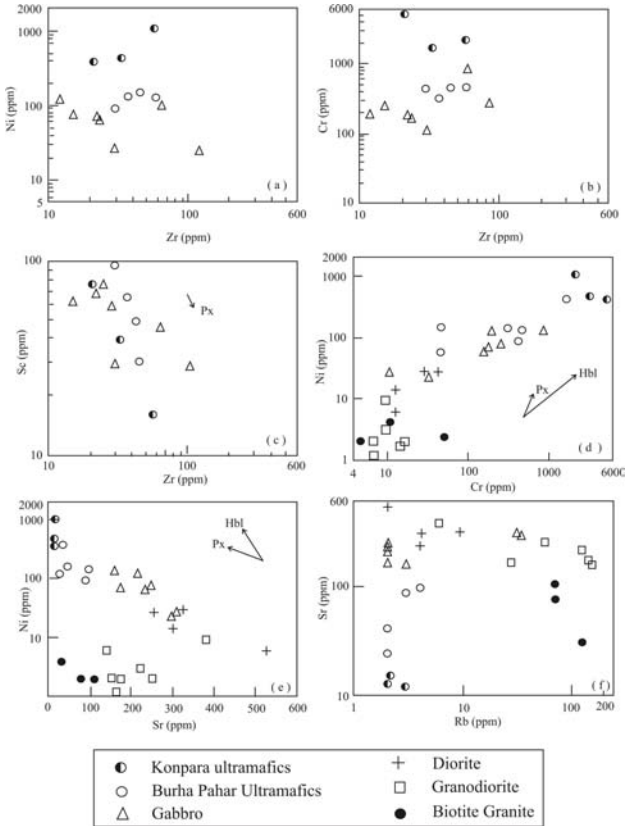

Fig.6.1. Plots of **(a)** Ni vs Zr, **(b)** Cr vs Zr, **(c)** Sc vs Zr, **(d)** Ni vs Cr, **(e)** Ni vs Sr and **(f)** Sr vs Rb for the ultramafic, mafic, dioritic, granodioritic and granitic rocks from Pathalgaon area. Arrow heads represent the fractionation trends of either pyroxene or hornblende from a magma with composition akin to hornblende gabbro.

samples at the periphery of the mafic bodies and their foliated character.

The mafic rocks are slightly enriched in LREE with $(La/Sm)_N$ ~ 1.05-4.70 and $(La/Yb)_N$ ~ 1.04-8.55. Their REE distribution pattern largely resembles EMORB (Fig 6.3a). Three of the samples have higher LREE proportions. Since the same samples have higher K and Rb, such discrepancies can be attributed to contamination. The REE distribution pattern of the ultramafics is largely similar to that of the gabbro except for sample B-52, which has a high $(La/Yb)_N$ value of 7.88 and also anomalously high Sm concentration, possibly attributed to contamination (Fig 6.3b).

The biotite granites are LREE enriched (with $(La/Yb)_N$ ~ 25.5-32.40, Fig 6.3c), while, granodiorites have widely varying REE patterns with $(La/Yb)_N$ values varying from 5.10 to 10.08 (Fig 6.3d). The diorites generally do not have any Eu-anomaly with the sole exception of sample B-15 that has a positive Eu-anomaly that can be attributed to plagioclase accumulation (Fig. 6.3d). In contrast, the negative Eu anomaly of all granodiorite samples is quite pronounced and can be explained through plagioclase fractionation with the exception of sample S-50(GT) that has a positive Eu anomaly that can be due to plagioclase accumulation.

Post Crystallization Element Mobility

Post crystallization metamorphic overprint can disturb trace elements systematics. However, loss on ignition for the studied gabbros is low (~ 2 wt %). Also, consistency in plots of Mg-no. vs mobile elements like K (Fig.5.3c) and Rb (Fig 5.3d) also indicate minimum post-crystallization trace element mobility with a few exceptions as reflected in the multi-element plots (Fig.6.2) and discussed in the preceding section. Limited ionic mobility is also evident in Zr vs Nb (Fig 6.4a), Zr vs Ce (Fig.6.4b) and Ce vs Nd (Fig. 6.4d) diagrams. Such consistent correlations prove that although LREE, K and Rb for a few samples from marginal parts of the pluton shows post crystallization / syn crystallization element mobility and contamination, at least the HFSE was largely immobile for bulk of the area during post-crystallization metamorphism and hence, can be suitably applied to decipher the tectonomagmatic history of the rock.

DISCUSSION

Petrogenesis

Source of mafic magma

In the Zr/Y vs Nb/Y binary plots most samples plot within the plume array as does EMORB, although, the Burha Pahar mafics are richer in Nb compared to Konpara (Fig. 7.1). A few plots, however, are discretely outside the array and represent the contaminated magmas as will be discussed in the subsequent section (Fig.7.1).

The general relative enrichment of Ba and Th compared to Rb and relative depletion of Nb cannot be explained by possible contamination from the adjoining granodiorite since the later is also enriched in Rb and would have led to Rb contamination (Fig. 6.2a & d). An alternative source of enrichment is, therefore, required. Low Nb and enriched La and Th in a mafic magma can be caused by any one of the following reasons: (1) prior mantle depletion of Nb (Niu and Batiza, 1997); (2) enrichment of Th and La relative to Nb in rutile saturated partial melts from dehydrating subducting slab (Elliott et al. 1997); (3) inheritance from subducting sediments (Plank, 2005; Hawkesworth et al. 1997) and (4) crustal differentiation followed by assimilation of upper crustal materials by mafic magma (Plank, 2005).

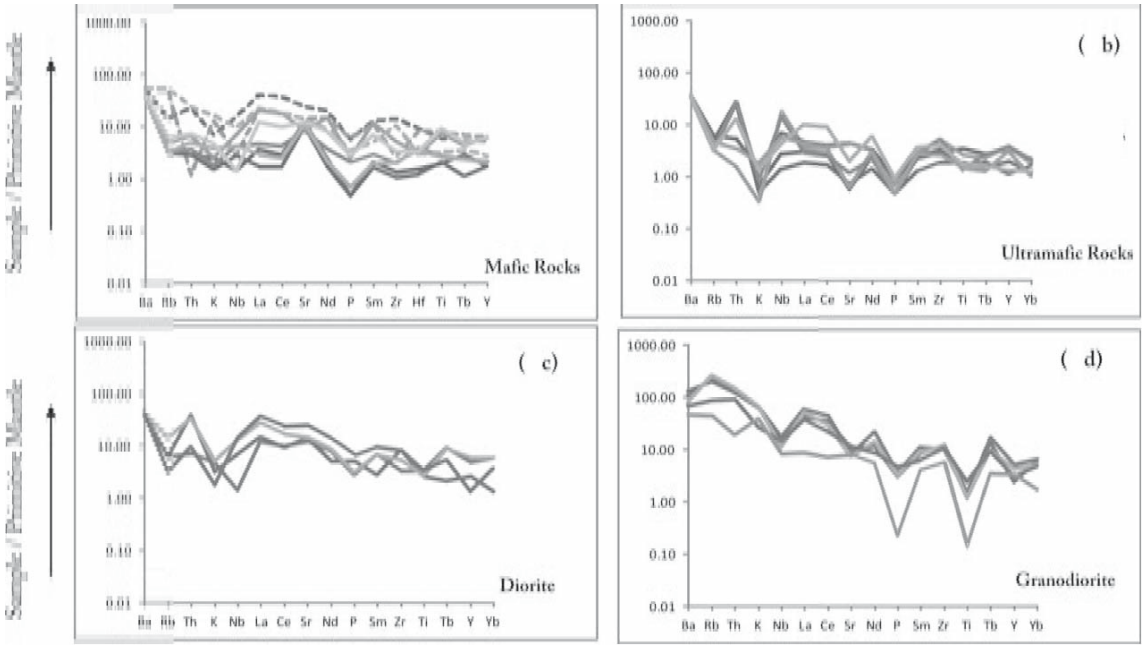

Fig.6.2. Primitive Mantle normalized multi-element variation diagrams for ultramafic, mafic, dioritic and granodioritic intrusives from Pathalgaon area, the plots characterized by dashed lines represent the contaminated samples collected from marginal parts of the pluton. The normalization factors as well as standard datasets for E-MORB, N-MORB and OIB (Oceanic Island Basalt) are after Sun and McDonough (1989).

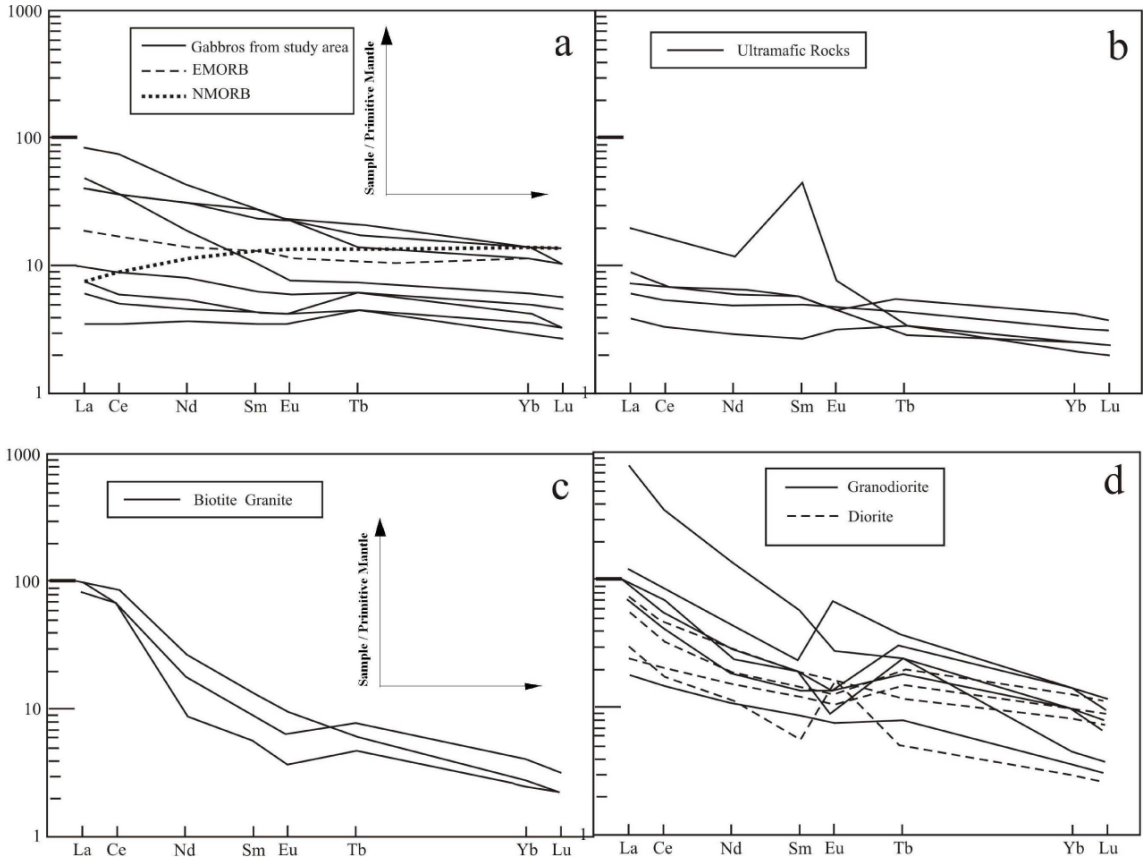

Fig 6.3. Primitive Mantle normalized REE variation diagrams for ultramafic, gabbroic, dioritic, granodioritic and granitic rocks from Pathalgaon area. Normalization values after Sun and McDonough (1989).

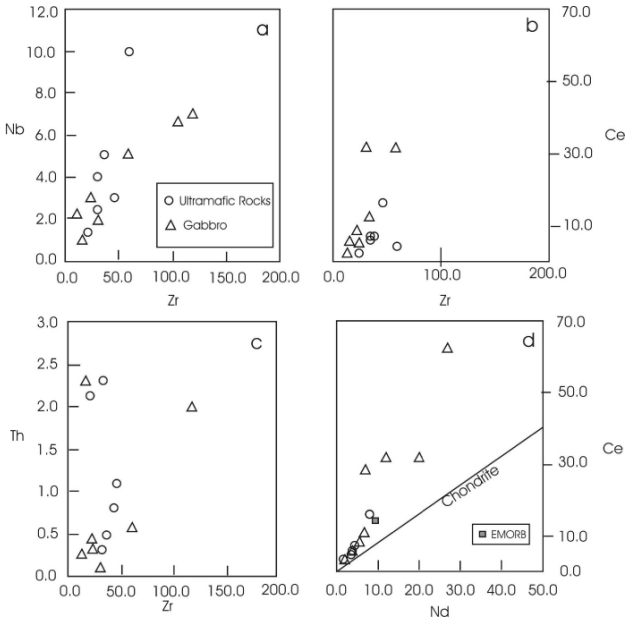

Fig 6.4. Plots of **(a)** Nb vs Zr, **(b)** Ce vs Zr, **(c)** Th vs Zr and **(d)** Ce vs Nd for the ultramafic and gabbroic rocks from Pathalgaon area (symbols as in Fig 5.1).

Lack of any good correlation between Ti and Th content of mafic rocks precludes rutile saturated slab melts. Assimilation of crustal material would definitely have led to the higher concentration of Rb compared to Ba. Therefore, effect of subducting dehydrating sediments over the mantle wedge appears to be the most plausible explanation for the observed trace element pattern. The fluid released from the dehydrating slab + sediment is normally hydrous with CO_2 and chloride. Such acidic medium will readily carry LILE like Rb, Sr and Ba at the expense of HFSE like Zr, Hf and Nb (Downes, 2001). But Rb is much less acidic and will thereby, under normal conditions, have higher concentration compared to Ba. Therefore, a preferential Ba enrichment over Rb has to be explained by Ba-enriched components in the subducted sediments.

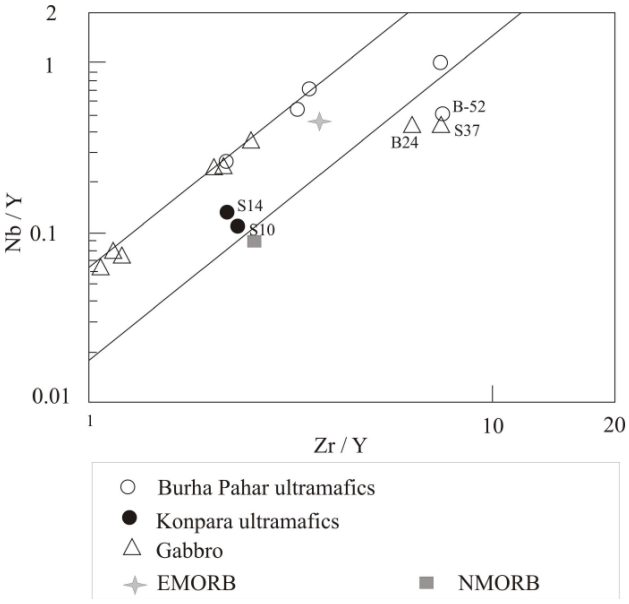

Fig 7.1. Zr/Y vs Nb/Y plume array plot (*after* Baksi, 2001) for mafic and ultramfic rocks from Pathalgaon area (also shown are the plots for EMORB and NMORB, bulk compositions from Sun and McDonough, 1989) (symbols as in Fig 5.1).

The Th/La ratio varies in samples from different mafic-ultramafic intrusive bodies with some having significantly higher Th concentration as compared to others. The Th variation is reflected in Zr vs Th plot, where, Konpara mafic and ultramafic rocks show a higher Th signature as compared to Burha Pahar body (Fig.6.4c). Also, variations in Ni, Cr, Sr and Mg between the different intrusive bodies can be attributed either to local heterogeneity in sub-continental lithospheric mantle source or to different degrees of local partial melting or both. Source variations are also apparent in Zr/Y vs Nb/Y binary plots where most samples plot within the plume array but the Burha Pahar mafics are richer in Nb compared to Konpara (Fig.7.1).

From the foregoing discussion, melting of a hybridized sub-continental lithospheric mantle wedge (with inputs from dehydrating / partially melting sediments from subducting plate) appears to be the most convenient source for the mafic-ultramafic rocks of Pathalgaon.

Fractionation of the Mafic-Ultramafic Rocks

Geothermobarometric data indicate that these rocks were crystallized from hydrous basaltic magma emplaced at mid-crustal depth (~ 5 kbar) at a temperature of ~ 1200 °C. Negative trend in MgO vs Al_2O_3 and initial negative trend in MgO vs CaO diagrams (Fig. 5.3a & b) could have resulted from accumulation of pyroxenes (Yang and Zhou, 2009). Trace element correlation diagrams also suggest pyroxene fractionation (~85% Cpx & 15% Opx) that resulted in the formation of ultramafic bands and lenses within the dominantly gabbroic complex. The bulk of the magma crystallized as hornblende-gabbro. Occasional preservation of remnant clinopyroxene within the cores of hornblende could have been possible due to the peritectic reaction involving near liquidus clinopyroxene in a primary hydrous melt:

Cpx + hydrous melt → Hbl… (Roberts et al. 2000)

Source and Evolution of Granite and Granodiorite

A compositional gap between the felsic and mafic series is well established in both major element Harker variation diagrams (Fig 5.1 and 5.2) and trace element distribution

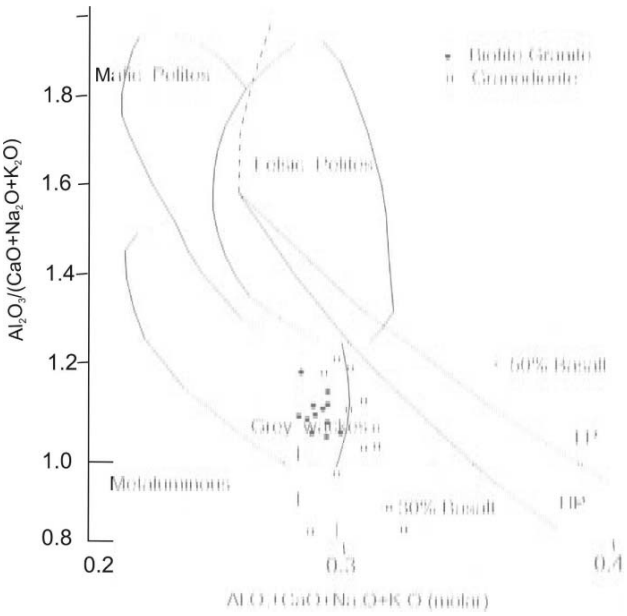

Fig 7.2. $Al_2O_3/(CaO + Na_2O + K_2O)$ vs molar Al_2O_3 + CaO + Na_2O + K_2O plots of biotite granite and granodiorite from Pathalgaon area; fields after Patino Douce, 1990.

patterns (Fig.6.1). The $ACNK_{molar}$ vs A/CNK_{molar} plot (Fig.7.2) of Patino Douce (1990) implies that the biotite granite was derived through partial melting of greywackes or equivalent feldspathic source, while, a larger distribution of granodiorite plots can be attributed to mixed mafic-feldspathic sources. Y+Nb vs Rb tectonic discrimination diagram attests that the granites and associated granodiorites are products of partial melting in a convergent setup (Fig.7.3, after Pearce et al. 1984).

Field relations, however, show a temporal gap between emplacement of granites and granodiorites. The granodiorites are closely associated with the mafic rocks with gradational and lobate margins between the two units and occasional presence of minor diorite with gradational contact with both the units (Fig. 1, 2b, 2c, 2d). Such features are indicative of coeval emplacement of mafic and granodioritic magmas. In contrast, the granite contains enclaves of metamorphosed and foliated mafic and pelitic rocks indicating that the terrain underwent deformation and low grade metamorphism prior to granite emplacement.

Magma Mingling: Diorite

Field evidences like occurrences of blebs and patches of mafic rock in granodioritic intrusives and vice versa (Fig.2c-d) and a general patchy composite appearance of the rocks occurring along the contacts of gabbros with granodiorite (Fig.2a) suggest marginal mingling and mixing of mafic and felsic magmas. The diorites occur very locally along the contacts of mafic and granodioritic rocks, with gradational contact with both the units. In the major element binary variation diagrams, the diorite plots extend between the granodiorites and the mafics (Fig.5.2), although their primitive mantle normalized multi element distribution pattern largely resembles the mafics. Such chemical signatures coupled with field relations suggest evolution of minor dioritic magmas through effective local mixing of gabbroic and granodioritic magmas. The contribution of effective magma mixing between coeval mafic and felsic end member magmas towards generation of hybrid magma is a much debated topic. Based on the viscosity of the individual magmas, crystallinity, relative viscosity, equilibrium temperature, mass fraction of the interacting magmas and time available for homogenization, several workers have shown that effective magma mixing is at best a local procedure (Huppert et al. 1984; Frost and Mahood, 1987; Johnston and Wyllie, 1988; Neves and Vauchez, 1995; Wiebe et al. 2004; Barbarin, 2005; Jayananda et al. 2009). The minor volume proportion of diorite compared to the volumes of granodiorite and gabbro is in corroboration to such contention.

The widespread occurrence of patchy/ variegated rocks along the contacts of mafic and granodioritic intrusives and the extreme anorthitic nature of the plagioclase in the leucocratic patches can be explained by contamination /

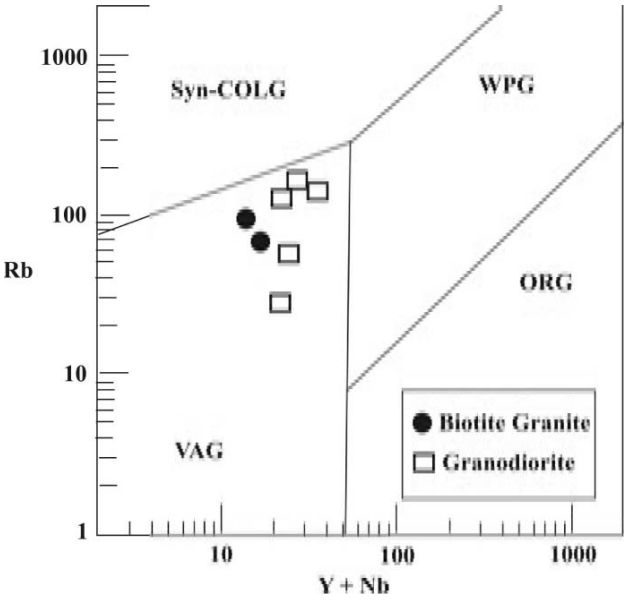

Fig 7.3. The Rb vs (Y + Nb) tectonic discrimination diagram (after Pearce et. al., 1984) showing fields of syn-collisional granites (syn-COLG), within-plate granites (WPG), volcanic-arc granites (VAG) and ocean-ridge granites (ORG). The biotite granite and granodirite samples from Pathalgaon area plot as VAG.

assimilation of Al_2O_3 and SiO_2 from the granodioritic magma. Philpotts (1994) has described the effects of magmatic assimilation over such compositional changes and development of anorthitic plagioclase in the marginal parts of mafic intrusive as a result of assimilation of siliceous and aluminous country rock by the intrusive magma. A similar reasoning involving marginal magma mixing can lead to development of the variegated rock with its high anorthitic plagioclase, where, the augitic component of the mafic melt interacts with Al_2O_3, SiO_2 and H_2O derived through mixing with granodioritic magma leading to the crystallization of primary anorthitic plagioclase and hornblende.

$$[Ca(MgFe)Si_2O_6]_{\text{mafic melt}} + [Al_2O_3 + SIO_2 + H_2O]_{\text{felsic melt}} \rightarrow CaAl_2Si_2O_6 + \text{Hornblende}$$

(*after* Philpotts, 1994)

Tectonic Significance

Many workers have questioned the separate identity of CGC and CITZ based on correlatable structures, shear zones and geochronological evidences (Jain et al. 1995; Chatterjee and Ghose, 2001; Acharya, 2003; Sanyal and Sengupta, 2012). From Ramakona Katangi mafic granulites exposed within the confines of Tan Shear Zone and Central Indian Shear in southern CITZ, Bhowmik and Roy (2003) deduced a compressional setup followed by extensional collapse leading to mafic magmatism in the form of sets of intrusive dykes. From Sm-Nd and Rb-Sr systematics, Roy et al (2006) deduced the age of this event to be ~ 1100 Ma with a younger 800-900 Ma Pan African overprint.

The present study area, forming a part of southern CGC, also represent a compressional setup as is established from tectonic discrimination diagrams of the granitoids (Fig 7.3) and other petrochemical fingerprints confirming that the mafic magma was derived from low degree partial melting of a hybrid sub-continental mantle wedge with possible component inputs from dehydrating / partially melting sediments from subducting plate. From Rb-Sr systematics, Singh and Krishna (2009) has established an age of ~ 1005±51 Ma for the grey granites from Kunkuri that are in physical continuity with the granites studied from Pathalgaon. The authors also established an younger 815± 51 Ma Pan African age for the pink granites locally present in Kunkuri. Combining their data with present petrographic and geochemical studies, and keeping in mind the possible temporal heterogeneity in evolution of different parts of a single orogen, it can be reasonably ascertained that the cogenetic felsic-mafic assemblage and the later granite from Pathalgaon was developed in a Grenvellian compressional setup with a possible late-Pan African overprint and thus conform that southern CGC and CITZ share a common geodynamic history from at least as early as Grenvellian orogeny.

CONCLUSION

The development of mafic-ultramafic-granodioritic-dioritic-granitic rock association of Pathalgaon in southern CGC can be summarized as follows:

1. Mafic magma produced through partial melting of hybridized sub-continental lithospheric mantle, possibly over a subduction zone.
2. Ascent and ponding of mafic magma at the base of crust leading to partial melting of the crustal rocks and generation of granodioritic magma
3. Simultaneous ascent and emplacement of granodioritic and hydrous mafic magmas at mid crustal levels and their intrusion into gneissic basement.
4. Marginal mingling and mixing of the magmas led to development of lobate and diffuse boundaries between the two units and locally resulted in diorite formation.
5. Deformation and metamorphism of the terrain leading to development of foliation and actinilitization of amphiboles near the marginal parts of the mafic intrusive and granodiorite.
6. Later emplacement of the regional granite, which, now contains enclaves of all these units.
7. Development of narrow anastomosing E-W trending shear zones that have affected all the lithounits.

Acknowledgements: This paper has been submitted with kind permission from the Deputy Director General, Geological Survey of India, Southern Region. We would like to thank Shri. Rabindra Moharana for his help in course of field work and subsequent sample preparation for chemical analyses. We thank Shri. Basab Chattopadhyay and Shri. Shyamal Sengupta for EPMA analysis. We are grateful to Sri. Sisir Dutta, Director (Retd.), Chemical Laboraotory, GSI, Nagpur, for kindly analyzing the samples for major and trace elements. Dr. Anjan Chatterjee from GSI, Nagpur has helped us in course of this work. We acknowledge his kind support. We also acknowledge the logistic support provided by Dr. Hanuma Prasad in course of our field work. Finally we are thankful to the reviewer for his critical review that has helped in improving the quality of the work.

References

ACHARYYA, S.K. (2003) A plate tectonic model for Proterozoic crustal evolution of Central Indian Tectonic Zone. Gondwana Res., v.7, pp.9-31.

ACHARYYA, A., ROY, S., CHAUDHURI, B.K., BASU, S.K., BHADURI, S.K. and SANYAL, S.K. (2006) Proterozoic rock suites along South Purulia Shear Zone, Eastern India: Evidence for rift related setting. Jour. Geol. Soc. India, v.68, pp.1069-1086.

ANDERSON, J.L. and SMITH, D.R. (1995) The effects of temperature and f_{O2} on the Al-in-hornblende barometer. Amer. Mineral., v.80, pp.519-559.

ARTH, J.G. (1976) Behaviour of trace elements during magmatic processes – a summary of theoretical models and their applications. Jour. Res. U.S. Geol. Surv., v.4, 41-47.

BAKSI, A.K. (2001) Search for a deep mantle component in mafic lavas using a Nb-Y-Zr plot. Canadian Jour. Earth Sci., v.38, no.5, pp.813-824.

BARBARIN, B. (2005) Mafic magmatic enclaves and mafic rocks associated with some granitoids on the Central Sierra Nevada batholiths, California: nature, origin and relations with the hosts. Lithos, v.80, pp.469-470.

BARKER, F. and ARTH, J.G. (1976) Generation of trondjhemite-tonalite liquids and Archaean bimodal trondjhemite-basalt suites. Geology, v.4, pp.596-600.

BHOWMIK, S.K. and ROY, A. (2003) Garnetiferous metabasites from the Sausar Mobile Belt: Petrology, P-T path and implications for the tectonothermal evolution of the Central Indian Tectonic zone. Jour. Petrol., v.44, no.3, pp.387-420.

CHATTERJEE, N. and GHOSE, N.C. (2011) Extensive early Neoproterozoic high-grade metamorphism in North Chotonagpur Gneissic Complex of the Central Indian Tectonic Zone. Gondwana Res., v.20, pp.362-379.

DOWNES, H. (2001) Formation and Modification of the Shallow Sub-Continental Lithospheric Mantle: a review of Geochemical Evidence from Ultramafic Xenolith Suites and Tectonically Emplaced Ultramafic Massifs of Western and Central Europe. Jour. Petrol., v.42, no.1, pp.233-250.

EARNST, W.G. and LIU, J. (1998) Experimental phase-equilibrium stud of Al- and Ti-contents of calcic amphibole in MORB—a semiquantitative thermobarometer. Amer. Mineral., v.83, pp.952-969.

ELLIOTT, T., PLANK, T., ZINDLER, A., WHITE, W. and BOURDON, B. (1997) Element transport from subducted slab to volcanic front at the Mariana arc. Jour. Geophys. Res., v.102, pp.14991-15019.

FROST, T.P. and MAHOOD, G.A. (1987) Field, chemical and physical constrains on mafic-felsic magma interaction in Lamarck granodiorite, Sierra Nevada, California. Geol. Soc. Amer. Bull., no.99, pp.272-291.

GHOSE, N.C. (1983) Geology,tectonics and evolution of the Chhotanagpur granite-gneiss complex, Eastern India. Recent Reserches in Geol., v.10, pp.211-247.

GHOSE, N.C. (1992) Chhotanagpur Gneiss-Granulite Complex, Eastern India: Present status and future prospect. Indian Jour. Geol., v.64(1), pp.100-121.

GHOSE, N.C. and MUKHERJEE, D. (2000) Chotanagpur Gneiss Granulite Complex, Eastern India – a kaleidoscope of global events. *In:* A.N. Trivedi, B.C.Sarkar, N.C.Ghose and Y.R.Dhar (Eds.), Geology and Mineral Resources of Bihar and Jharkhand, Platinum Jubilee Commemorative Volume, Indian School of Mines, Dhanbad, Inst. Geoexpl. Environ. Monograph 2, Patna, pp.33-58.

GHOSE, N.C., MUKHERJEE, D. and CHATTERJEE, N. (2005) Plume generated Mesoproterozoic mafic-ultramafic magmatism in the Chotanagpur Mobile Belt of Eastern Indian Shield Margin. Jour. Geol. Soc. India, v.66. no.6, pp.725-740.

HAWKESWORTH, C. J., TURNER, S. P., MCDERMOTT, F., PEATE, D. W. and VAN CALSTEREN, P. (1997) U–Th isotopes in arc magmas: implications for element transfer from the subducted crust. Science, v.276, pp.551-555.

HOLLAND, T. and BLUNDY, J. (1994) Non-ideal interactions in calcic amphiboles and their bearing on amphibole-plagioclase thermometry. Contrib. Mineral. Petrol., v.116, pp.433-447.

HOSSAIN, I., TSEUNAGE, T., RAJESH, M.H., CHEN, B. and ARAKAWA, Y. (2007) Palaeoproterozoic U-Pb SHRIMP zircon age from basement rocks in Bangladesh: a possible remnant of the Columbia supercontinent. C.R.Geoscience, v.339, pp.979-986.

HUPPERT, H.E. and SPARKS, R.S.J. (1988) The generation of granitic magmas by intrusion of basalt into continental crust. Jour. Petrol., v.29, pp.599-624.

IRVINE, T.N. and BARAGAR, W.R.A. (1971) A guide to geochemical classification of the common volcanic rocks. Canad. Jour. Earth Sci., v.8, pp.523-548.

JAIN, S.C., NAIR, K.K.K. and YEDEKAR, D.B. (1995) Geology of the Son-Narmada-Tapti Lineament Zone in Central India. *In*: Geoscientific Studies of the Son-Narmada-Tapti Lineament Zone. Geol. Surv. India Spec. Publ., No.10, pp.1-154.

JAYANANDA, M., MIYAZAKI, T., GIREESH, R. V., MAHESHA, N. and KANO, T. (2009) Synplutonic mafic dykes from late Archaean granitoids in the eastern Dharwar craton, southern India. Jour. Geol. Soc. India, v.73, pp.117-130.

JOHNSON, M.C. and RUTHERFORD, M.J. (1989) Experimental calibration of the Al-inhornblende geobarometer with application to Long Valley caldera (California). Geology, v.17, pp.837-844.

JOHNSTON, A.D. and WYLLIE, P.J. (1988) Interaction of granitic and basaltic magmas: experimental observations on contamination processes at 10 kbar with H_2O. Contrib. Mineral. Petrol., v. 98, pp.352-362.

KRETZ, R. (1983) Symbols for rock forming minerals. Amer. Mineral., v.68, pp.77-279.

KUMAR, S., RINO, V. and PAL, A.B. (2004) Typology and Geochemistry of microgranular enclaves in Malanjkhand granitoids, Central India. Jour. Geol. Soc. India, v.64, pp.277-292.

KUMAR, S., PIERU, T., RINO, V. and LYNGODH, V.C. (2005) Microgranular enclaves in Neoproterozoic granitoids of South Khasi hill, Meghalaya Plateau, Northeastern India: field evidence of interacting coeval mafic and felsic magmas. Jour. Geol. Soc. India, v.65, pp.629-633.

KUMAR, S. and RINO, V. (2006) Mineralogy and Geochemistry of microgranular enclaves in Palaeoproterozoic Malanjkhand granitoids, Central India: evidence of magma mingling mixing and chemical equilibriation. Contrib. Mineral. Petrol., v.152, pp.591-609.

KUMAR, S. (2010) Mafic to hybrid microgranular enclaves in Ladakh batholiths, northwestern Himalaya: Implications on calc alkaline magma chamber processes. Jour. Geol. Soc. India, v.76, pp.5-25.

LINDSLEY, D. H. (1987) Pyroxene Thermometry. Amer. Mineral., v.68(5-6), pp.477- 493.

MAHADEVAN, T.M. (2002) Geology of Bihar and Jharkhand. Geological Society of India, Bangalore, 563p.

MAHADEVAN, T.M. (2008) Precambrian Geological and Structural Features of the Indian Peninsula. Jour. Geol. Soc. India, v.72, pp.35-56.

MAZUMDAR, S.K. (1988) Crustal evolution of the Chhotanagpur gneissic complex and the Mica Belt of Bihar. *In:* D. Mukhopadhyay (Ed.), Precambrian of the Eastern Indian Shield. Mem. Geol. Soc. India, no.8, pp.49-84.

MAZUMDAR, S.K. and CHATTERJEE, S. (1990) A note on the geotectonic status of the Tamar-Porapahar fracture zone near the southern edge of the CGGC. Seminar on Tectono-magmatic evolution of CGGC. Bull.Geol. Min.Metall. Soc. India, v.56, p.12.

Neves, S.P. and Vauchez, A. (1995) Successive mixing and mingling of magmas in a plutonic complex of northeast Brazil. Lithos, v.34, pp.275-299.

NIU, Y. and BATIZA, R. (1997) Trace element evidence from seamounts for recycled oceanic crust in the eastern Pacific mantle. Earth Planet. Sci. Lett., v.148, pp.471– 483.

PATINO DOUCE, A. E. (1990) What do experiments tell us about the relative contributions of crust and mantle to the origin of granitic magmas? *In*: A. Castro, C. Fernandez and J.L. Vignerese (Eds.), Understanding Granites: Integrating new and classical techniques. Geol. Soc. London Spec. Publ., v.118, pp.55-75.

PEARCE, J.A., HARRIS, N.B.W. and TINDLE, A.G. (1984) Trace element discrimination diagrams for the tectonic interpretation of the granitic rocks. Jour. Petrol., v.25, pp.956-983.

PECCERILLO, R. and TAYLOR, S.R. (1976) Geochemistry of Eocene calc-alkalic volcanic rocks from the Kastamanu area, northern Turkey. Contrib. Mineral. Petrol., v.58, pp.63-81.

PHILPOTTS, A.R. (1994) Principles of Igneous and Metamorphic Petrology. Prentice Hall, 258p.

PLANK, T. (2005) Constraints from Thorium/Lanthanum on Sediment Recycling at Subduction Zones and the Evolution of the Continents. Jour. Petrol., v.46, no.5, pp.921-944.

PITCHER, W.S. (1991) Synplutonic Dykes and mafic enclaves. *In*: J. Didier and B. Barbarin (Eds.), Enclaves and Granite Petrology, Developments in Petrology, v.13, Elsevier, Amsterdam, pp.383-391.

ROBERTS, M.P., CHRISTIAN, P., CLEMENS, J.D. and PAQUETTE, J-L. (2000) Petrogenesis of Mafic to Felsic Plutonic Rock Associations: the Calc-alkaline Querigut Complex, French Pyrenees. Jour. Petrol., v.41, no.6, pp.809-844.

ROY, A. and CHAKRABORTY, K. (2008) Precambrian Mafic-Ultramafic magmatism in Central Indian Suture Zone. Jour. Geol. Soc. India, v.72, pp.123-140.

ROY, A., KAGAMI. H., YOSHIDA, M., ROY, A., BANDYOPADHYAYA, B.K., CHATTOPADHYAY, A., KHAN, A.S., HUIN, A.K. and PAL, T. (2006) Rb-Sr and Sm-Nd dating of different metamorphic events from the Sausar Mobile Belt, Central India: Implications for Proterozoic crustal evolution. Jour. Asian Earth Sci., v.26, pp.61-76.

ROY, A. and PRASAD, H.M. (2003) Tectonothermal events in Central Indian Tectonic Zone (CITZ) and its implication in Rhodinian crustal assembly. Jour. Asian Earth Sci., v.22, pp.115-129.

SANYAL, S. and SENGUPTA, P. (2012) Metamorphic evolution of the Chotanagpur Granite Gneissic Complex (CGGC) of Eastern Indian Shield: Current Status. Geol. Soc. London Spec. Publ. "Palaeoproterozoic of India" (in press)

SCHMIDT, M.W. (1992) Amphibole composition in tonalite as a function of pressure: an experimental study at 650ºC. Contrib. Mineral. Petrol., v.110, pp.304-310.

SHARMA, R. (2009) Cratons and Fold Belts of India. Springer-Verlag, 304p.

SINGH, Y. and KRISHNA, V. (2009) Rb-Sr Geochronology and Petrogenesis of Granitoids from Chhotanagpur Granite Gneiss Complex of Raikera-Kunkuri Region, Central India. Jour. Geol. Soc. India, v.74, pp.200-208.

SRIVASTAVA, R.K. and CHALAPATI RAO, N.V. (2007) Petrology, geochemistry and tectonic significance of Paleoproterozoic alkaline lamprophyres from the Jungel Valley, Mahakoshal supracrustal belt, Central India. Mineral. Petrol., v.89, pp.189-215.

SUN, S.S. and MCDONOUGH, W.F. (1989) Chemical and isotopic systematic of oceanic basalts: implications for mantle composition and processes. Jour. Geol. Soc. London. v.42, pp.313-345.

THOMAS, W.M. and ERNST, W.G. (1990) The aluminium content of hornblende in calcalkaline granitic rocks: A mineralogic barometer calibrated experimentally to 12 kbars. *In:* R.J. Spencer and I-M. Chou (Eds.), Fluid-mineral interactions: A tribute to H. P. Eugster. Geochem. Soc. Spec. Publ., v.2, pp.59-63.

WIEBE, R. A., MANON, M. R., HAWKINS, D.P. and MCDONOUGH, W. F. (2004) Late-stage mafic injection and thermal rejuvenation of the Vinalhaven granite, Coastal Maine. Jour. Petrol., v.45, pp.2133-2153.

WIEBE, R.A. (1991) Commingling of contrasted magmas and generation of mafic enclaves in granitic rocks. *In:* J. Didier and B. Barbarin (Eds.), Enclaves and Granitic Petrology, Elsevier, Amsterdam, 625p.

YANG, S.H. and ZHOU, M.F. (2009) Geochemistry of the ~430 Ma Jingbulake mafic-ultramafic intrusion in Western Xinjiang, NW China: Implications for subduction related magmatism in the South Tianshan orogenic belt. Lithos, v.113, pp.259-273.

(Received: 14 July 2011; Revised form accepted: 5January 2012)